Interannual Variability of the U.S. Summer Precipitation Regime with Emphasis on the Southwestern Monsoon

R. W. HIGGINS AND K. C. MO

Climate Prediction Center, NOAA/NWS/NCEP, Washington, D.C.

Y. YAO

Research and Data Systems Corporation, Greenbelt, Maryland

(Manuscript received 16 May 1997, in final form 5 December 1997)

ABSTRACT

Relationships between the interannual variability of the U.S. summer precipitation regime and the intensification, weakening, or changes in position of the climatological-mean circulation features that organize this regime are examined. The focus is on the atmospheric conditions over the conterminous United States relative to wet and dry monsoons over the southwestern United States. The onset of the monsoon in this region, which typically begins in early July, is determined using an index based on daily observed precipitation for a 32-yr (1963–94) period. Composites of observed precipitation and various fields from the National Centers for Environmental Prediction–National Center for Atmospheric Research Reanalysis for wet and dry monsoons are used to show that the interannual variability of the summer precipitation regime closely mimics the seasonal changes associated with the development of the North American monsoon system.

The warm season precipitation regime is characterized by a continental-scale precipitation pattern consisting of an out-of-phase relationship between the Southwest and the Great Plains/Northern Tier and an in-phase relationship between the Southwest and the East Coast. This pattern is preserved for both wet and dry monsoons, but the Southwest is relatively wetter and the Great Plains are relatively drier during wet monsoons. Wet (dry) monsoons are also associated with a stronger (weaker) upper-tropospheric monsoon anticyclone over the western United States, consistent with changes in the upper-tropospheric divergence, midtropospheric vertical motion, and precipitation patterns. The intensity of the monsoon anticyclone over the western United States appears to be one of the most fundamental controls on summertime precipitation downstream over the Great Plains.

Evidence is presented that the interannual variability of the U.S. warm season precipitation regime is linked to the season-to-reason ''memory'' of the coupled atmosphere–ocean system over the eastern tropical Pacific. In particular, it is shown that SST anomalies in the eastern Pacific cold tongue and precipitation anomalies in the intertropical convergence zone, present during the winter and spring preceding the monsoon, are linked via an anomalous local Hadley circulation to the warm season precipitation regime over the United States and Mexico. Wet (dry) summer monsoons tend to follow winters characterized by dry (wet) conditions in the Southwest and wet (dry) conditions in the Pacific Northwest. This association is attributed, in part, to the memory imparted to the atmosphere by the accompanying Pacific SST anomalies.

1. Introduction

The social and economic impacts of large-scale hydrologic anomalies, such as the 1993 Midwest flood and the 1988 Midwest drought, are considerable. These events remind us that the year-to-year variability of warm season precipitation is large. In semiarid regions, such as Arizona and New Mexico, the interannual variability tends to be even larger in relation to the seasonal mean rainfall.

Meteorologists have long referred to a ''southwest monsoon'' over Arizona and New Mexico, which typically begins in early July. It is now well known that this monsoon is the northernmost portion of a more extensive region of heavy precipitation that first develops over southern Mexico during the spring and then spreads northward along the western slopes of the Sierra Madre occidental (e.g., Douglas et al. 1993; Stensrud et al. 1995). Heating over the elevated terrain of Mexico and the western United States plays a major role in the development and evolution of this monsoon, in a manner similar to what is observed with the Tibetan Plateau and the South Asian Monsoon (e.g., Tang and Reiter 1984) and with the Bolivian Antiplano and the South American Monsoon (e.g., Johnson 1976).

Of potentially greater significance for the understanding of the warm season precipitation regime of

Corresponding author address: Dr. R. W. Higgins, Analysis Branch, Climate Prediction Center, NOAA/NWS/NCEP, W/NP52, 4700 Silver Hill Rd., Stop 9910, Washington, DC 20233.
E-mail: wd52wh@sgi85.wwb.noaa.gov

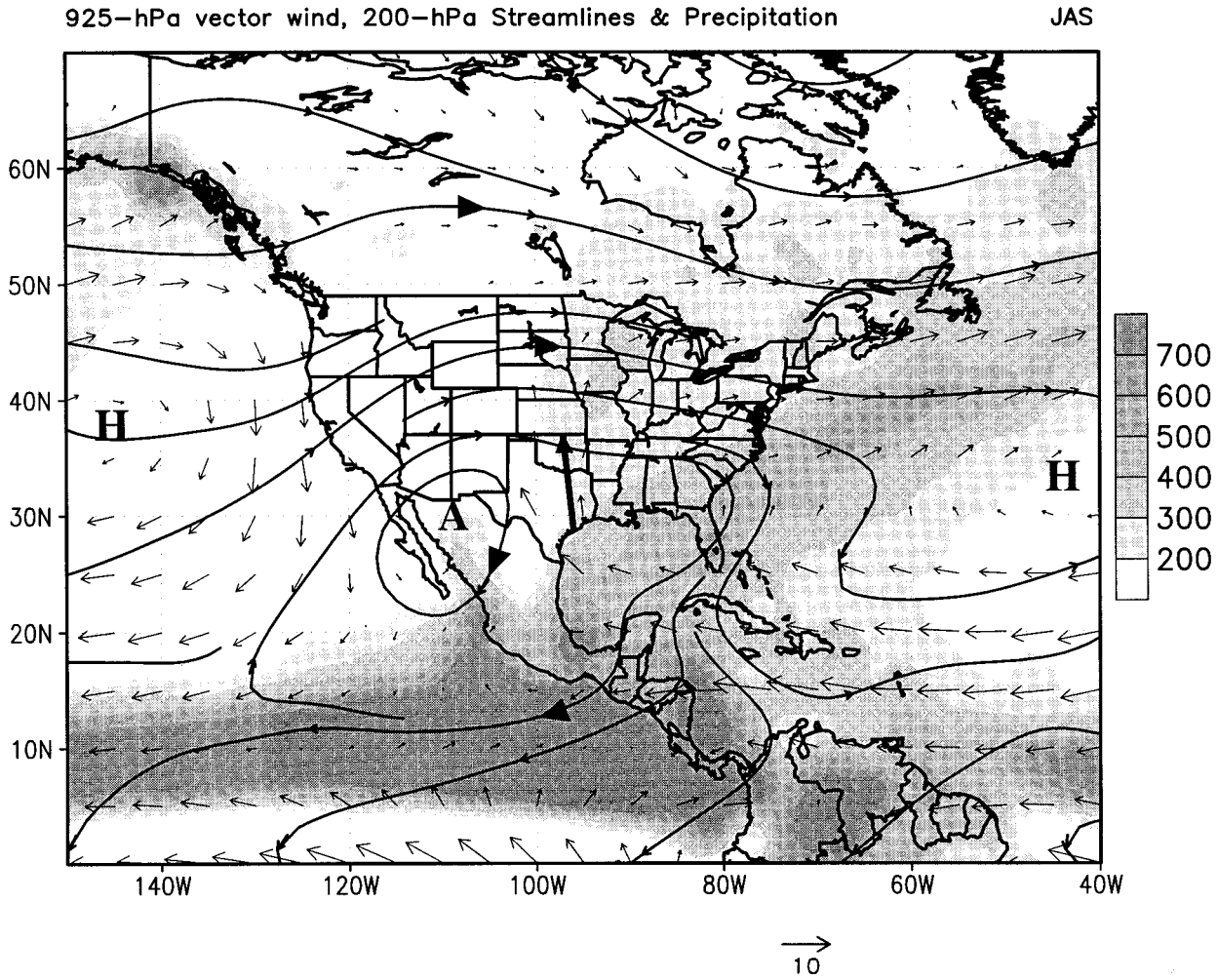

FIG. 1. Mean (JAS 1979–95) 925-hPa vector wind, 200-hPa streamlines, and merged satellite estimates and station observations of precipitation (shading). Circulation data are taken from the NCEP–NCAR Reanalysis archive. The position of the North American Monsoon Anticyclone is indicated by A. The Bermuda and North Pacific subtropical high pressure centers are indicated by H. Precipitation amounts are in mm. The approximate location of the Great Plains low-level jet is indicated by the heavy solid arrow.

North America is the fact that the North American monsoon system (hereafter NAMS), of which the Mexican monsoon is the primary upward branch, affects much of the United States and Mexico (e.g., Higgins et al. 1997b; hereafter HYW97). Over the United States there is evidence of a continental-scale mode in the warm season precipitation pattern consisting of an out-of-phase relationship between the Southwest and the Great Plains/Northern Tier and an in-phase relationship between the Southwest and the East Coast. Recent studies by HYW97 and Okabe (1995) have shown that phase reversals in this pattern are related to the development and decay of the NAMS. A description of the life cycle of the NAMS in terms of development, mature, and decay phases, and a literature review are given in HYW97. For convenience, the schematic summarizing key elements of the NAMS during July–September (Fig. 1 in HYW97) is reproduced as Fig. 1. The schematic emphasizes the controlling influences of the large-scale low-level flow around the subtropical high pressure centers (indicated by ''H''), the large-scale upper-level flow around the North American Monsoon anticyclone (indicated by ''A''), and the nature of the warm season precipitation regime.

This study is an attempt to extend our earlier work by diagnosing the interannual variability of the U.S. warm season precipitation regime. Our goal is to show that there is a continental-scale mode of interannual variability that is similar in character to the changes associated with the development of the NAMS as discussed in HYW97. We also argue that drought (flood) episodes in the central United States during the summer are likely associated with what may be broadly char-

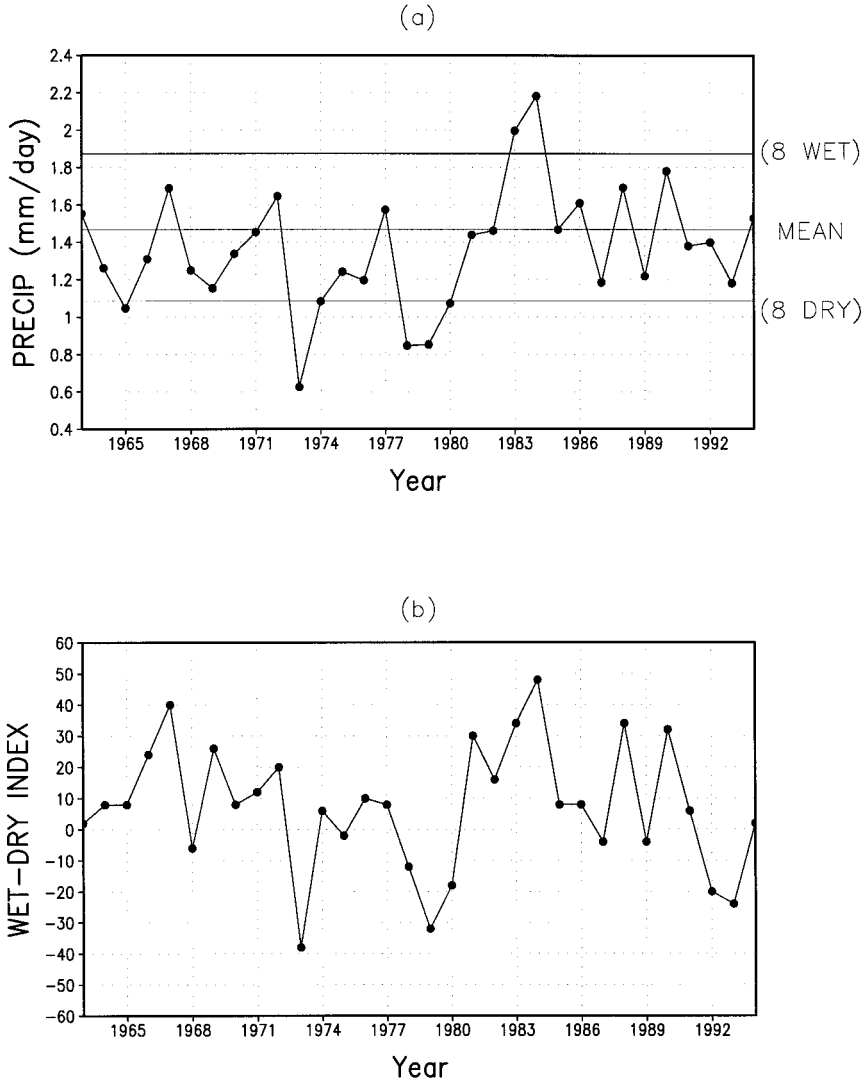

FIG. 2. Mean daily (a) precipitation (units: mm day^{-1}) and (b) wet–dry index over Arizona and New Mexico (32°–36°N, 112.5°–107.5°W) for the 90-day period (day +1–day +90) after monsoon onset.

acterized as an amplification (weakening) of the NAMS and, in particular, the monsoon ridge over the western United States.

The basic approach will be to identify ''wet'' and ''dry'' monsoons in Arizona and New Mexico using the objective approach first defined in HYW97 together with observed daily precipitation for a 32-yr (1963–94) period and then to compare and contrast the hydrologic conditions and atmospheric circulation features over the conterminous United States in each case. This study also includes some preliminary analysis of relationships between warm season precipitation over North America and changes in 1) the eastern Pacific intertropical convergence zone (ITCZ); 2) the local Hadley circulation; 3) the sea surface temperature, especially in the vicinity of the eastern tropical Pacific cold tongue; and 4) the equatorial subsurface thermal structure of the ocean. Specific links between the NAMS and the ENSO cycle will not be discussed per se. The relative roles of boundary forcing (SST and soil moisture) of seasonal to interannual variability, the location and maintenance of heat sources and sinks and their relationship to the hydrologic cycle, and the mechanisms responsible for tropical–extratropical interactions will be considered in follow-on studies.

Section 2 describes the datasets and the precipitation index used to classify wet and dry monsoons. Features of the U.S. summer precipitation regime for wet and dry monsoons are discussed in section 3. Related changes in the eastern Pacific ITCZ cold tongue complex are described in section 4. A summary and discussion are given in section 5.

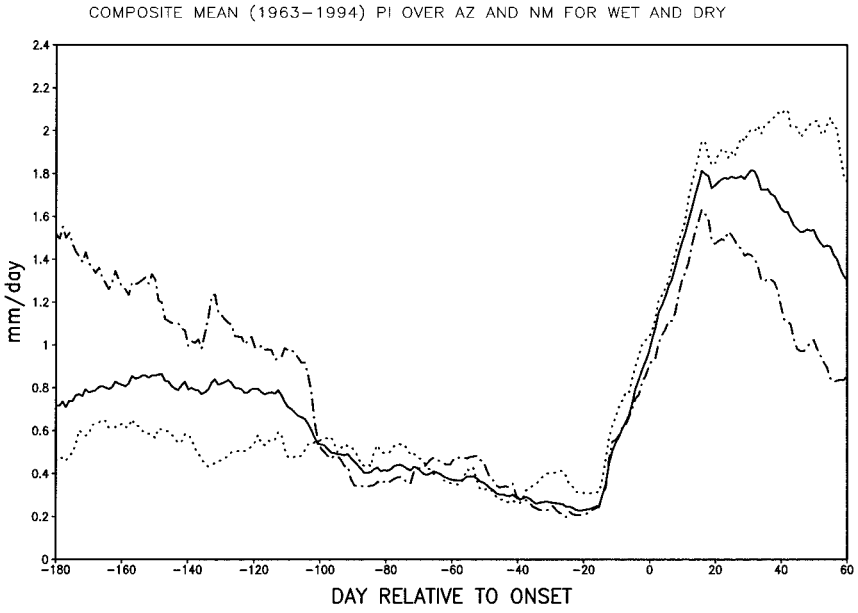

FIG. 3. Composite evolution of the 30-day running mean precipitation index (PI) (units: mm day^{-1}) over Arizona and New Mexico for wet monsoons (dotted line), dry monsoons (dot-dashed line), and all (1963–94) monsoons (solid line). The average date of monsoon onset is 1 July for wet monsoons, 11 July for dry monsoons, and 7 July for all monsoons (defined as day 0 in each case).

2. Data analysis

a. Datasets

The dataset used to study atmospheric circulation features associated with wet and dry monsoons is the National Centers for Environmental Prediction–National Center for Atmospheric Research (NCEP–NCAR) Reanalysis (Kalnay et al. 1996), which currently spans the period 1968–96. We note, however, that the reanalysis project will ultimately provide at least 40 yr (1957–1996+) of global-gridded fields. The NCEP–NCAR assimilation system consists of the NCEP Medium Range Forecast spectral model and the operational NCEP Spectral Statistical Interpolation (Parrish and Derber 1992) with the latest improvements (Kalnay et al. 1996). The assimilation is performed at a horizontal resolution of T62 and 28 sigma levels in the vertical with seven levels below 850 hPa. In this study we utilize the reanalysis winds and specific humidity, which are instantaneous fields available every 6 h, and several diagnostic fields (e.g., precipitation and evaporation) that are generated by the GCM's physical parameterizations. In the NCEP system, the precipitation and evaporation fields are based on a 6-h forecast valid at the initial synoptic time. Moisture transport was computed directly from winds and specific humidity on the respective model sigma levels (Mo and Higgins 1996). All reanalysis fields are averaged to daily values prior to compositing as described below.

In order to diagnose the interannual variability of observed precipitation over the United States we exploit a gridded hourly precipitation database for the conterminous United States developed by Higgins et al. (1996a; hereafter HJY 96). These analyses were developed from station observations obtained from the National Weather Service (NWS) Techniques Development Laboratory. The time domain covers the period 1 January 1963–31 December 1994. The analyses were gridded to a horizontal resolution of 2° lat × 2.5° long. We note that in this study the term ''rainfall'' is equivalent to measurable precipitation.

In order to explore relationships between the variability of the warm season precipitation regime over the conterminous United States and rainfall anomalies elsewhere, we employ a global precipitation dataset obtained from a merge of rain gauge observations [obtained via the Climate Anomaly Monitoring System (CAMS) of the Climate Prediction Center] and satellite-derived precipitation estimates. The satellite estimates are generated by the outgoing longwave radiation precipitation index (OPI) technique (Xie and Arkin 1998), which are merged with rain guage data via a method adapted from Xie and Arkin (1996). For convenience, in the remainder of this paper we will refer to the global precipitation dataset as CAMS/OPI. The data were gridded to a horizontal resolution of 2° lat × 2.5° long. This dataset is available on a monthly basis for the period 1979–95, which implies that wet (dry) monsoons prior to 1979 are not included in composites. However, comparisons to the precipitation dataset of HJY96 are used for verification of the precipitation patterns over the conterminous United States.

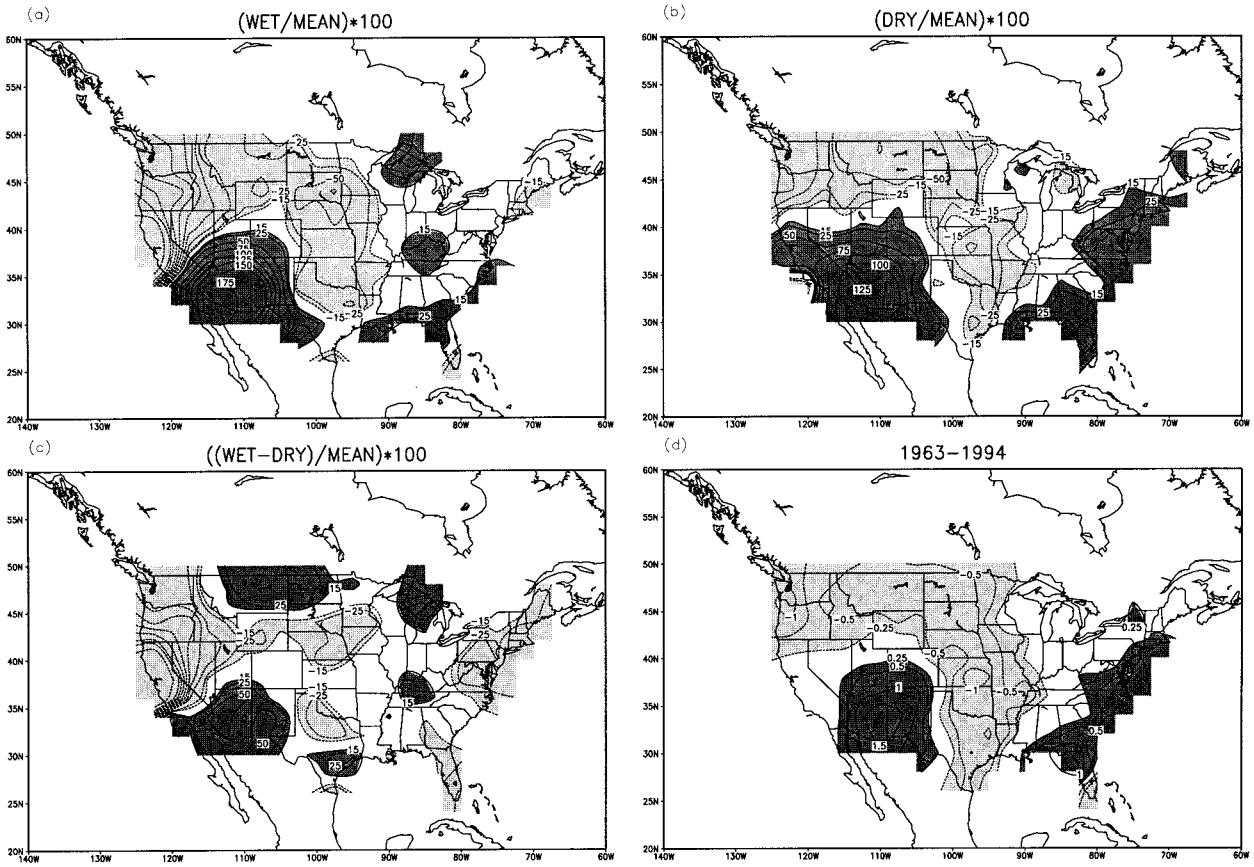

FIG. 4. Maps of observed precipitation (units: mm day^{-1}) represented as the mean difference between the 45-day period after onset (day 0 to day +44) and the 45-day period before onset (day −45–day −1) for (a) wet, (b) dry, (c) wet–dry, and (d) 1963–94. In (a) and (b) the differences are represented as the percent departure from normal for the Jun–Aug 1963–94 period. In (a)–(c) the contour interval is 25% (to which the 15% contour has been added) and values greater than 15% (less than −15%) are shaded dark (light). In (d) the contour interval is 0.5 mm day^{-1} (to which the 0.25 mm day^{-1} contour has been added) and values greater than 0.25 mm day^{-1} (less than −0.25 mm day^{-1}) are shaded dark (light).

Sea surface temperature data used in section 4b were obtained from the historical reconstruction of Smith et al. (1996); these data are gridded to a horizontal resolution of 2° lat × 2° long and are available for the period 1950–95. The data used to describe the depth of the 20°C isotherm and the subsurface ocean temperatures are derived from an ocean data assimilation system, which assimilates oceanic observations into an oceanic GCM (Ji et al. 1995); these data were available for the period 1980–95. To the extent possible, the climatology for all of the datasets above (including the reanalysis) is from the 1979–95 base period monthly means.

b. Classification of wet and dry monsoons

HYW97 defined a precipitation index (PI) over Arizona and New Mexico based on the gridded daily precipitation of HJY96 that we will apply here to determine wet and dry monsoons. The PI is obtained by averaging daily accumulations of observed precipitation at each grid point of the rectangular region (32°–36°N, 112.5°–107.5°W) over Arizona and western New Mexico. Histograms of the mean (1963–94) daily rainfall (and the 5-day running mean) during summer at each grid point over the southwestern United States (see Fig. 2 of HYW97) show that all of the grid points used for the PI exhibit rapid onset of monsoon rainfall around the beginning of July. Monsoon onset dates were determined using the resulting time series and a threshold crossing procedure. The PI magnitude and duration criteria used were +0.5 mm day^{-1} and for 3 consecutive days, respectively; the monsoon onset date for each year occurs when the selection criteria are first satisfied after 1 June. Composite evolution fields for 1963–94 are obtained by averaging over all of the monsoons relative to the day when the PI first satisfies the threshold criteria; this day is designated as the onset day, or day 0. Note that by realigning the time series in this way we are not performing a simple average based on calendar day. Based on this analysis the average date of the monsoon onset for the period 1963–94 is 7 July.

The PI was used to classify individual years as wet

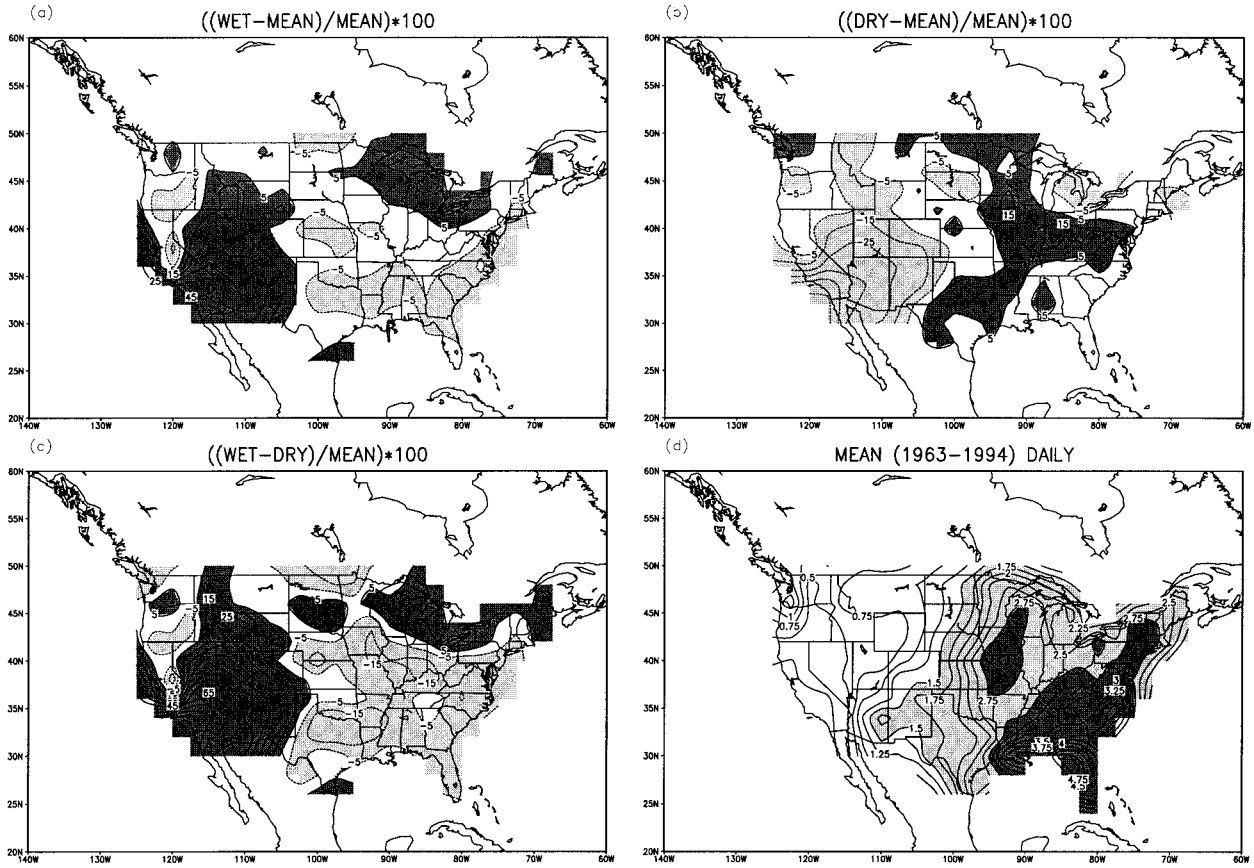

FIG. 5. Maps of observed precipitation (units: mm day^{-1}) represented as the composite mean (day +1–day +90) for (a) wet−mean, (b) dry−mean, (c) wet–dry, and (d) 1963–94. In (a)–(c) the differences are represented as the percent departure from normal for the Jun–Aug 1963–94 period. In (a)–(c) the contour interval is 10% (to which the 5% contour has been added) and values greater than 5% (less than −5%) are shaded dark (light). In (d) the contour interval is 0.25 mm day^{-1} and values greater than 1.5 mm day^{-1} (greater than 2.75 mm day^{-1}) are shaded light (dark).

or dry for the period 1963–94 by averaging daily precipitation for the 90-day period after monsoon onset (Fig. 2a). If we order the individual values on Fig. 2a from largest to smallest and use the top 25% to classify wet monsoons and the bottom 25% to classify dry monsoons, then we find wet monsoons in 1967, 1972, 1977, 1983, 1984, 1986, 1988, and 1990; and dry monsoons in 1965, 1969, 1973, 1974, 1978, 1979, 1980, and 1993. The remaining 50% (16 yr) are considered normal years. This classification gives a reasonable separation between wet and dry monsoons; mean values for the 90-day period after onset are 1.77 mm day^{-1} for wet, 0.98 mm day^{-1} for dry, and 1.37 mm day^{-1} for all monsoons. The average date of onset is 1 July for wet monsoons and 11 July for dry monsoons.

Based on this classification we note that the 1988 Midwest drought occurred just prior to a wet Southwest monsoon, which had one of the earliest onset dates (24 June) in the 1963–94 period. The 1993 Midwest flood occurred in the same summer as a dry Southwest monsoon, which had the latest onset date (3 August) in the 1963–94 period. We note that a similar (but not identical) classification of wet and dry monsoons is obtained when we use July–September rainfall rather than the 90-day period after monsoon onset. In general we find that keying to the monsoon onset date using the daily data produces sharper features in the precipitation composites, and so composites based on daily data are presented in section 3a. Some of the observational datasets, including the CAMS/OPI and the SST, are available on a monthly basis; when these datasets are used, we use the classification above to produce seasonal composites (see sections 3b and section 4).

The PI above is based on total amounts of daily precipitation. As described in Okabe (1995), the use of total amounts has two important limitations. One is that trace amounts of precipitation are often neglected, which is important if one is concerned with the percentage of days on which precipitation occurs. Second, totals are often biased toward large events. For example, heavy convective rains that occur during the summer can produce total rainfall amounts in one day that match or exceed long-term monthly averages. To determine whether such biases exist in our data, and hence in the

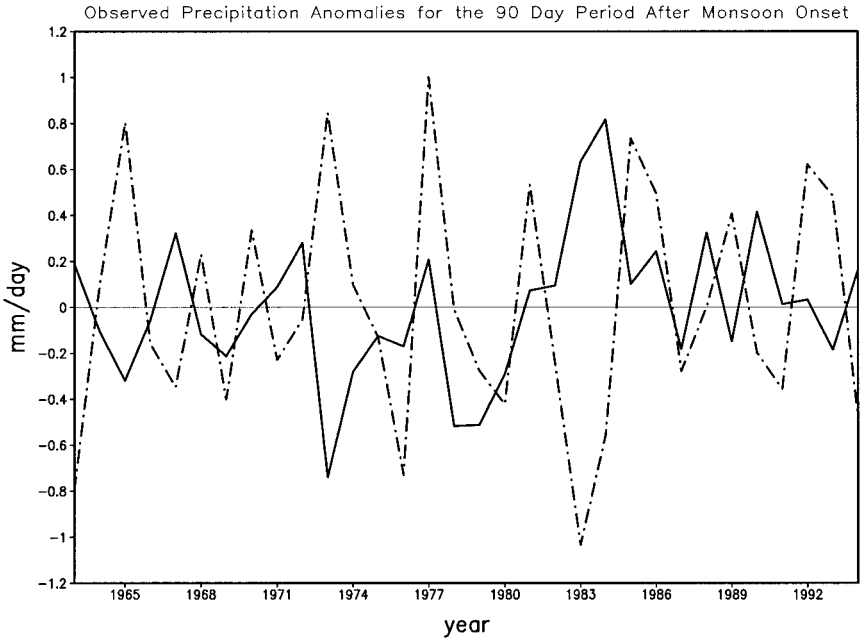

FIG. 6. Areal average observed precipitation anomalies (units: mm day^{-1}) for the 90-day period after monsoon onset from the PI region (solid line) and from the central plains (34°–42°N, 100°–92.5°W)(dot-dashed line).

classification of wet and dry years, we apply the wet–dry index of Okabe (1995). As described in his work, the first step is to recode daily precipitation events, whether large or small, as ''1s.'' Then all days without precipitation are recoded as ''−1s.'' Because we are working with gridded precipitation averaged over a box, exact zeros are unlikely (Okabe worked with station data); for this reason we define measurable precipitation as anything greater than 0.05 mm day^{-1}. All missing data are recorded as zeros. Thus a running sum of the recoded data, the wet–dry index, increases during wet periods and decreases during dry periods. The final index number is a measure of the dryness or wetness over the period of interest. Okabe (1995) used 1-yr periods but here we are interested in the 90-day period after monsoon onset (Fig. 2b). Comparison of Figs. 2a and 2b shows that, in general, there is a good correspondence between wet years and high values of the wet–dry index and between dry years and low values of the index. This comparison suggests that our precipitation totals are not severely biased toward trace or heavy amounts.

The composite evolution of the PI for wet, dry, and all (1963–94) monsoons is shown in Fig. 3. In both wet and dry years the onset of the Southwest monsoon rains is clearly evident, just as it is in the composite based on all years; HYW97 note that the compositing scheme based on the PI may make the monsoon onset appear to be abrupt because it is keyed to synoptic as well as climate variability. Wet monsoons are characterized by a much longer period of heavy rainfall after onset than dry ones. Interestingly, the composite evolution also shows that wet (dry) summer monsoons are preceded by dry (wet) conditions relative to the mean during the preceding winter (roughly days −180 to −100); this relationship is explored further in section 4c. Also note that there is very little difference during the preceding spring (roughly, days −100 to −20) (see section 4a).

3. Features of the U.S. summer precipitation regime

In this section we examine features of the U.S. summer precipitation regime during wet and dry monsoons as defined in section 2b. In addition to composites of precipitation and tropospheric circulation for wet and dry monsoons, we also present mean fields in order to provide a proper reference for interpreting departures from the mean. When appropriate, difference maps between wet and dry composites are also presented.

a. Precipitation

HYW97 showed that the mean summer precipitation regime over the United States is characterized by an out-of-phase relationship between precipitation in the Southwest and in the Great Plains/Northern Tier and an in-phase relationship between precipitation in the Southwest and the East Coast. A map of the composite mean observed precipitation represented as the difference between the 45-day period after onset (day 0 to day +44) and the 45-day period before onset (day −45 to day −1) for all (1963–94) monsoons (Fig. 4d) shows the

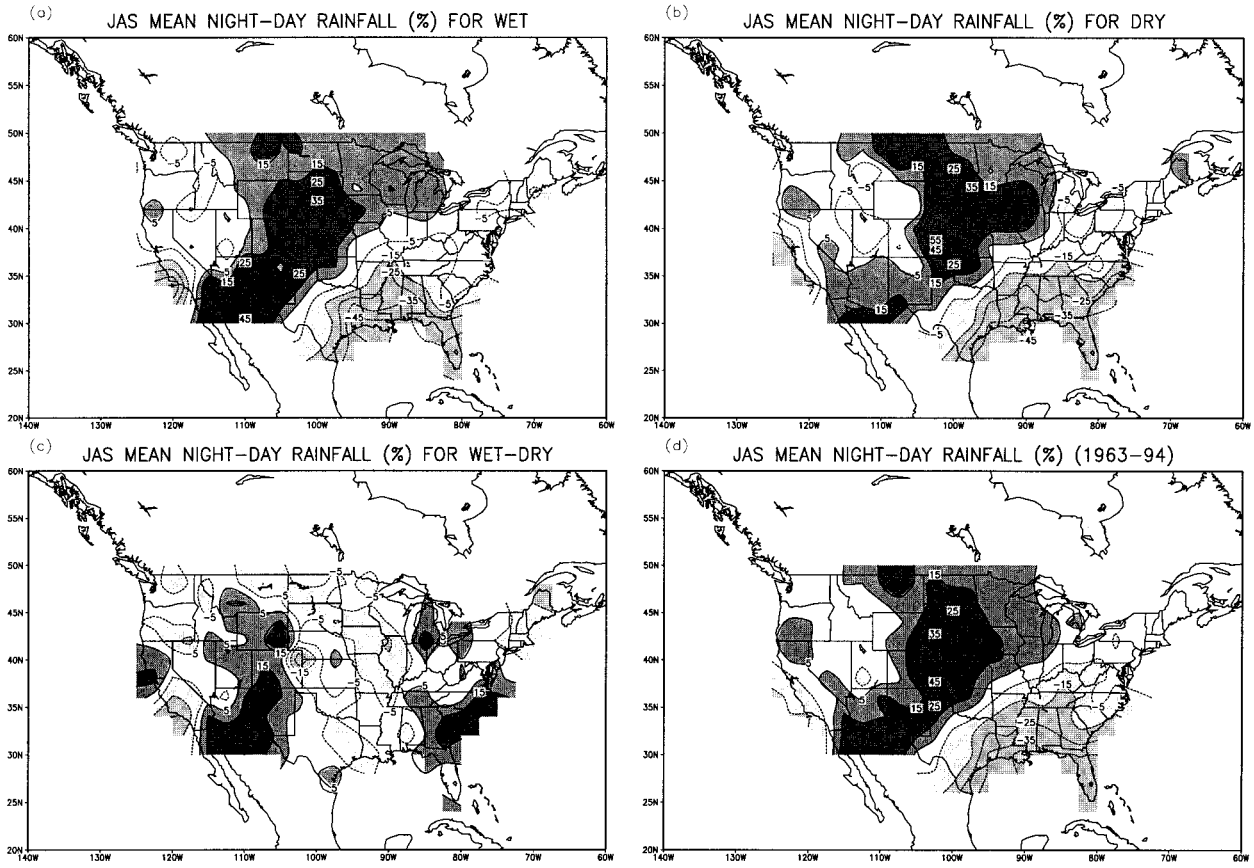

FIG. 7. Mean JAS precipitation difference between nighttime (0000–1200 UTC accumulation) and daytime (1200–0000 UTC accumulation) expressed as a percentage of the mean (1963–94) daily precipitation for (a) wet, (b) dry, (c) wet–dry, and (d) 1963–94. In (a)–(d) the contour interval is 10%, the zero contour is omitted, and values greater than 5% (less than −5%) are shaded dark (light).

continental-scale precipitation pattern. Previous studies have linked the onset of the summer rains over northern Mexico and the southwestern United States to a decrease of rainfall over the Great Plains (e.g., Mock 1996; Tang and Reiter 1984; Douglas et al. 1993; A. Douglas 1997, personal communication; Mo et al. 1997). This continental-scale pattern appears to be strongly modulated by the intensity of the monsoon anticyclone over the western United States.

The interannual variability of this precipitation pattern closely mimics the changes associated with the development of the monsoon. Maps of the composite-mean observed precipitation represented as the difference between the 45-day period after onset and the 45-day period before onset for wet (Fig. 4a) and dry (Fig. 4b) monsoons show that the continental-scale precipitation pattern is preserved in each case; here the composites are represented as the percent departure from normal for the June–August (JJA) 1963–94 period. In each composite the Southwest is wetter after onset, but there is more precipitation during wet monsoons (Fig. 4c). The Great Plains and Northern Tier are drier after onset as a result of the strengthened and expanded mid- and upper-tropospheric monsoon high (see section 3b), but wet monsoons are associated with a relatively drier Great Plains compared to dry monsoons (Fig. 4c). It is important to note, however, that increases in the amplitude of the diurnal cycle of precipitation (e.g., Wallace 1975), in the frequency of occurrence of the nocturnal Great Plains low-level jet (e.g., Bonner 1968; Bonner and Paegle 1970; Mitchell et al. 1995; Helfand and Schubert 1995; Augustine and Caracena 1994; Higgins et al. 1997a), and in mesoscale convective activity (e.g., Maddox 1980) *keep the region relatively wet compared to the drier winter months.* Over portions of the Northern Plains and the Northeast the differences between wet and dry monsoons are roughly as large as they are in the Southwest (Fig. 4c), emphasizing the potential impact of monsoon variability on ground water and irrigation for these regions. The large differences along the immediate West Coast should be discounted because the mean precipitation during the summer months is quite small in this region.

One remarkable aspect of Fig. 4 is the cellular nature of the precipitation anomaly patterns for all types of monsoons (i.e., wet, dry, normal). This seems to suggest that U.S. agriculture is virtually immune to entire failure. Possible large-scale controls on the spatial variation

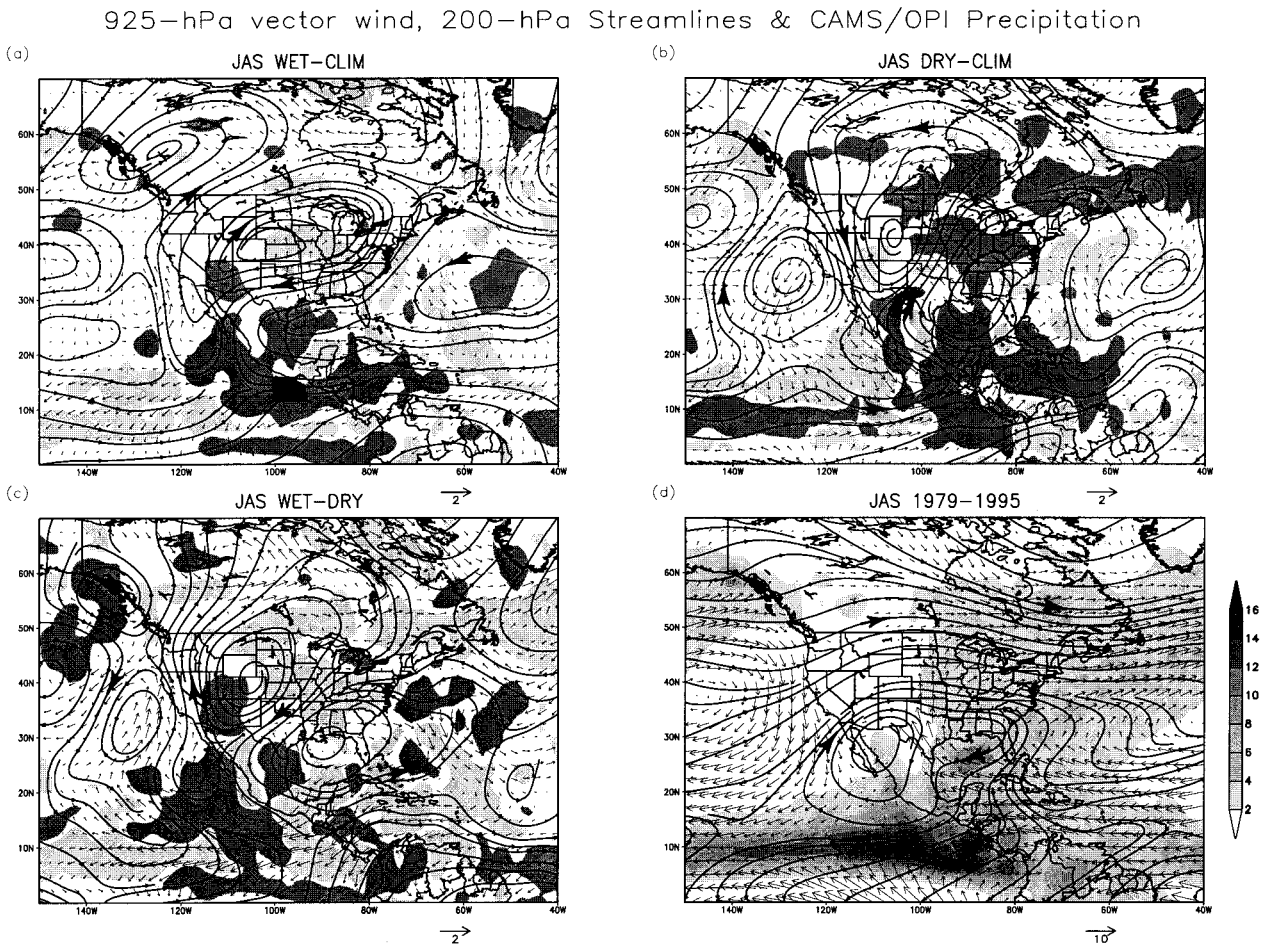

FIG. 8. JAS 925-hPa wind vectors (units: m s^{-1}), 200-hPa streamlines, and CAMS/OPI precipitation (units: mm day^{-1}) for (a) wet, (b) dry, (c) wet–dry, and (d) JAS 1979–95. A topography mask has been applied to the 925-hPa winds. In (a) and (b) the fields are represented as departures from mean (JAS 1979–95) values. In (a)–(c) the standard vector length is 2 m s^{-1}, and in (d) the standard vector length is 10 m s^{-1}. In (a)–(c), precipitation values greater than 0.25 mm day^{-1} (less than −0.25 mm day^{-1}) are shaded dark (light).

and intensity of this precipitation pattern are discussed in the following sections.

Further examination of the period after onset (day +1 to day +90; roughly July–September), in which the wet and dry composites are first represented as departures from mean (1963–94) daily values and then expressed as the percent departure from normal (Figs. 5a,b), clearly shows that wet (dry) monsoons are associated with enhanced (suppressed) rainfall over the southwestern United States. A difference map (Fig. 5c) shows that rainfall during wet monsoons exceeds that of dry monsoons by more than 50% over Arizona and western New Mexico; again, the large values along the immediate West Coast should be discounted. Over the Southwest the maximum precipitation occurs in August, but wet monsoons are characterized by several months (June–October) of above-normal rainfall while dry monsoons are associated with several months (June–September) of below-normal rainfall. During wet monsoons much of the central Great Plains, lower Mississippi Valley, and East Coast are drier than normal while the Great Lakes and southern Texas are wetter than normal (Fig. 5a). During dry monsoons much of the Mississippi Valley, Ohio Valley, and mid-Atlantic States are wetter than normal (Fig. 5b).

The relationship between rainfall in the Southwest and over the Great Plains is explored further in Fig. 6, which shows a comparison of precipitation anomalies [departures from the mean (1963–94) daily precipitation for the 90-day period after monsoon onset] from the PI (solid line) and from the central Great Plains (34°–42°N, 100°–92.5°W; dot-dashed line). An out-of-phase relationship is clearly evident in most years; the out-of-phase relationship holds for all wet monsoons (except 1977 and 1986) and all dry monsoons (except 1969 and 1980). When we key to persistent wet and dry events in the central plains, we reproduce the phase reversal between the Southwest and the Great Plains (Mo et al. 1997).

The interannual variability of the *diurnal cycle* of

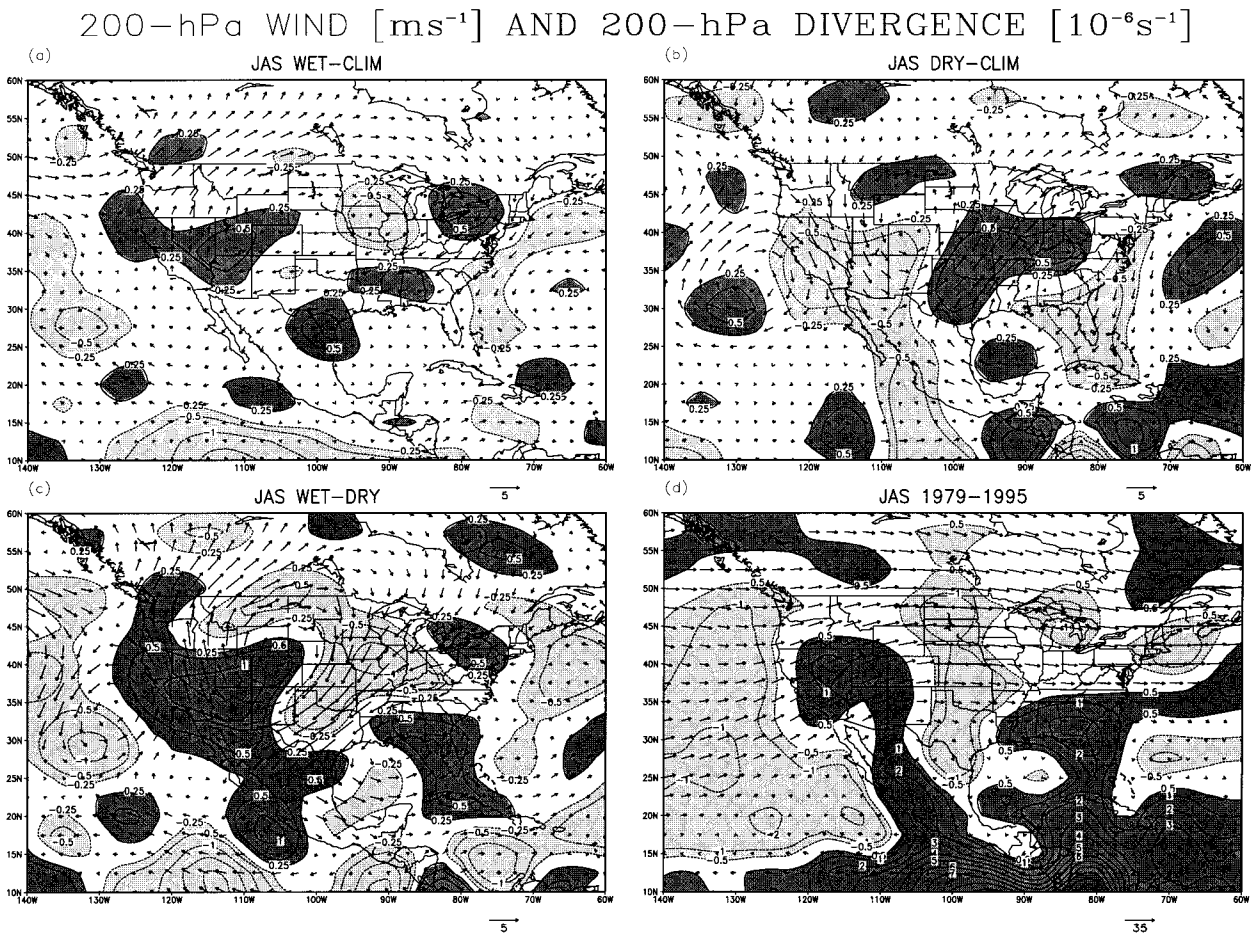

FIG. 9. JAS 200-hPa wind (units: m s^{-1}) and 200-hPa divergence (units: 10^{-6} s^{-1}) for (a) wet, (b) dry, (c) wet–dry, and (d) 1979–95. In (a) and (b) the fields are represented as departures from mean (JAS 1979–95) values. In (a)–(d) the contour interval is 0.5×10^{-6} s^{-1} [the 0.25×10^{-6} s^{-1} contour has been added in (a)–(c)] and the dark (light) shading indicates positive (negative) values. In (a)–(c) the standard vector length is 5 m s^{-1} and in (d) the standard vector length is 35 m s^{-1}.

observed precipitation is also similar to changes in the continental-scale precipitation pattern due to the development of the monsoon. Examination of the mean July–September (JAS 1963–94) difference between nighttime (0000–1200 UTC) and daytime (1200–0000 UTC) precipitation (Fig. 7d) shows that nighttime rainfall exceeds daytime rainfall over most of the Great Plains and the desert Southwest. A commensurate decrease in nighttime rainfall is found along the Gulf Coast. Between the plains and the southeast, much smaller differences between nighttime and daytime rainfall are observed in a narrow region from central Texas to the Great Lakes. Wet (dry) monsoons are associated with an amplified (suppressed) diurnal cycle in the SW monsoon region and a suppressed (enhanced) diurnal cycle over much of the Great Plains and Midwest (Figs. 7a,b); we note that the values have been normalized by mean daily values so that they may be compared. Interestingly, the difference map (Fig. 7c) resembles the continental-scale precipitation pattern discussed in Fig. 4. We note that additional details on diurnal variations in precipitation over the conterminous United States are found in Wallace (1975) and Higgins et al. (1996a).

b. Tropospheric circulation and moisture

The mean large-scale low-level (925-hPa) flow over the southern United States and Mexico is strongly influenced by the subtropical highs, with brisk southerlies over the southern Great Plains (reflecting the Great Plains low-level jet) and northwesterlies west of Baja California (reflecting the Baja jet) (Fig. 8d); note that a topography mask has been applied to the 925-hPa winds. The NCEP–NCAR Reanalysis does not capture the southerly component in the lower tropospheric winds over the northern Gulf of California and southern Arizona found in observational studies (e.g., Baden-Dangon et al. 1991; Douglas et al. 1993) because the horizontal resolution is too coarse (e.g., Schmitz and Mullen 1996; HYW97). The winds at 200 hPa (Fig. 8d shows streamlines and Fig. 9d shows vector winds) are characterized by weak easterlies over the deep Tropics

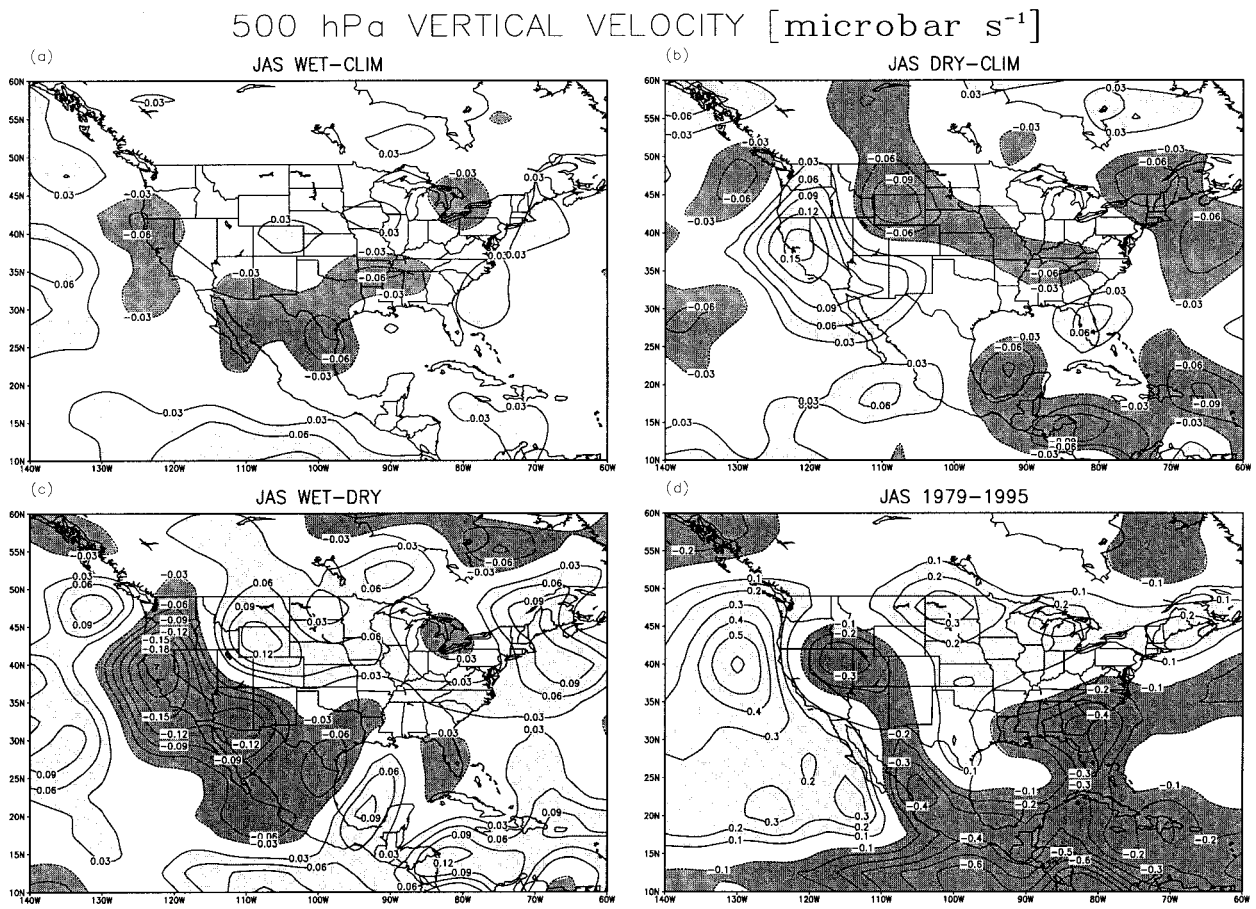

FIG. 10. JAS 500-hPa vertical velocity (units: μb s^{-1}) for (a) wet, (b) dry, (c) wet–dry, and (d) 1979–95. In (a) and (b) the fields are represented as departures from mean (JAS 1979–95) values. In (a)–(c) the contour interval is 0.03 μb s^{-1}, and values greater than 0.03 μb s^{-1} (less than -0.03 μb s^{-1}) are shaded light (dark). In (d) the contour interval is 0.1 μb s^{-1}, and values greater than 0.1 μb s^{-1} (less than -0.1 μb s^{-1}) are shaded light (dark).

(the easterlies are stronger in the midtroposphere; see Fig. 9b in HYW97), widespread westerlies poleward of roughly 35°N, and an anticyclonic circulation centered over northwestern Mexico. The mean upper-tropospheric divergence (Fig. 9d) and midtropospheric vertical motion (Fig. 10d) fields are broadly consistent with the distribution of warm season precipitation (Fig. 8d) as represented in the CAMS/OPI precipitation product (see section 2a). Upper-tropospheric divergence in the vicinity and south of the monsoon anticyclone coincides with deep easterly flow, midtropospheric upward motion, and monsoon rainfall. In contrast, upper-tropospheric convergence over the Great Plains coincides with midtropospheric downward motion and suppressed rainfall. The precipitable water (not shown) indicates abundant moisture over the tropical eastern Pacific, Gulf of California, Baja California, western Mexico, and the eastern half of the United States; similar moisture distributions have been discussed by numerous authors (Starr et al. 1965; Hales 1974; Hagemeyer 1991; Douglas et al. 1993; Negri et al. 1994; Schmitz and Mullen 1996; HYW97).

During wet monsoons the large-scale low-level flow shows small departures from the mean (Fig. 8a), but changes in the upper-tropospheric circulation (Figs. 8a and 9a) are dramatic and consistent with changes in the continental-scale precipitation pattern (Fig. 8a). The upper-tropospheric monsoon anticyclone is much stronger than normal and shifted to the northeast of its climatological-mean position (Figs. 8a, 9a). Along the southern tier of states and in the Southwest the anomalous upper-tropospheric easterly flow (Fig. 9a) and midtropospheric upward motion (Fig. 10a) are consistent with enhanced monsoon precipitation over Arizona and New Mexico (Fig. 8a). During dry monsoons the upper-level flow is characterized by a much weaker monsoon anticyclone that is shifted somewhat to the south, with a large-scale cyclonic anomaly centered over the central High Plains. Comparison of the upper-tropospheric anomaly pattern in Fig. 8b to the climatology (Fig. 8d)

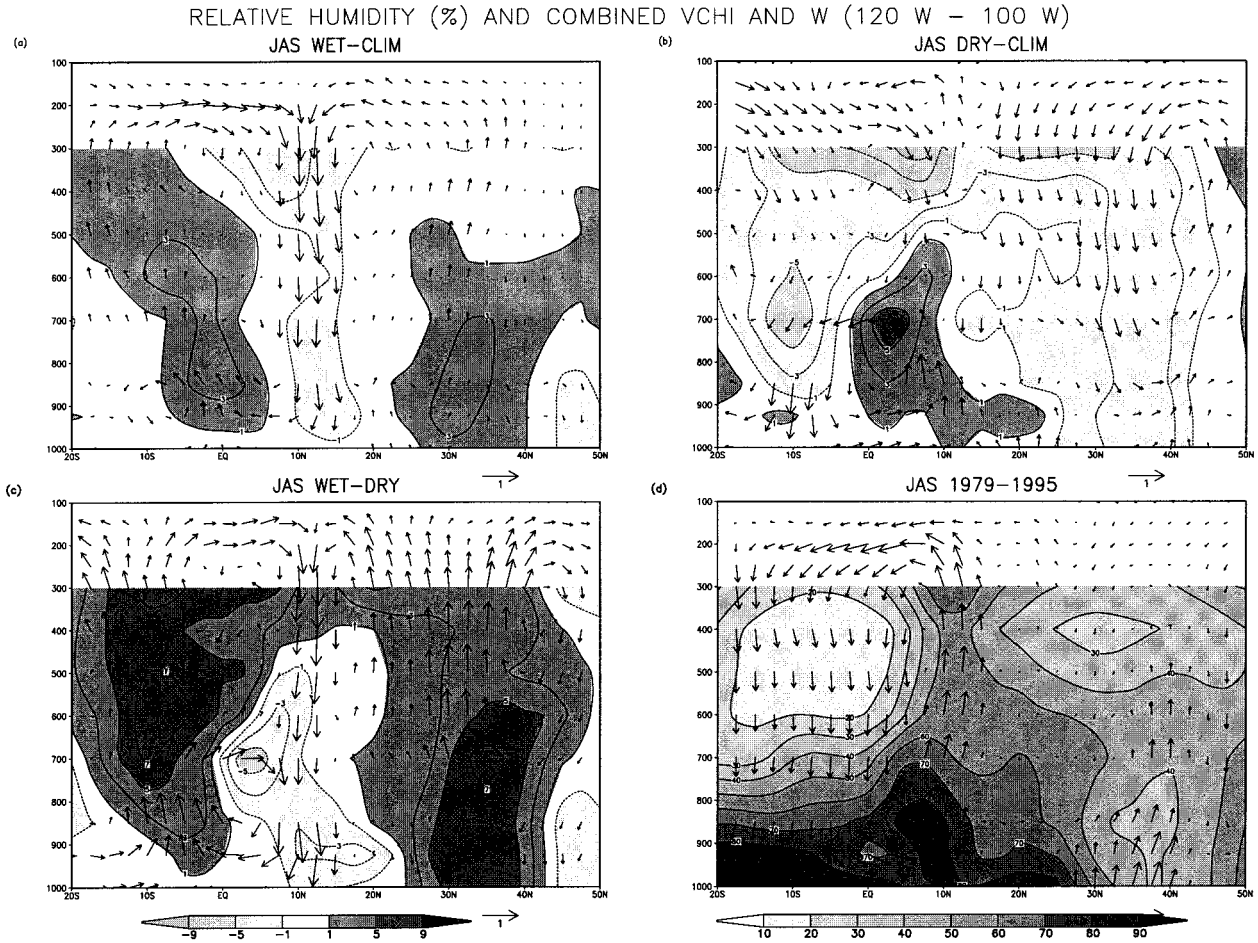

FIG. 11. Latitude–pressure cross sections in the band 120°–100°W of the JAS relative humidity (units: percent) and combined divergent meridional wind and pressure vertical velocity (vectors) for (a) wet, (b) dry, (c) wet–dry, and (d) 1979–95. In (a) and (b) the fields are represented as departures from mean (JAS 1979–95) values. In (a)–(c) the contour interval is 2% and values greater than 1% (less than −1%) are shaded dark (light). In (d) the contour interval is 10%. In (a)–(c) the standard vector length is 1 m s^{-1} and in (d) the standard vector length is 5 m s^{-1}.

indicates that dry monsoons are associated with a broad flattening of the upper-tropospheric ridge consistent with an increased zonal component of the flow. In the Southwest the anomalous upper-tropospheric northwesterly flow (Fig. 9b) and midtropospheric subsidence (Fig. 10b) are consistent with suppressed precipitation. These results are consistent with those of Carleton et al. (1990), who showed that a northward displaced monsoon anticyclone is associated with wetter summers in Arizona and that a southward displaced monsoon anticyclone is associated with drier summers in Arizona. We note that the precipitation composites from CAMS/OPI and HJY96 are quite similar over the conterminous United States (not shown).

Enhanced upper-tropospheric northerly flow (Fig. 9a) and weak midtropospheric subsidence (Fig. 10a) to the north and east of the monsoon anticyclone during wet monsoons are consistent with suppressed precipitation extending in an arc from the Great Plains to the southeast. Increased upper-level southwesterly flow (Fig. 9b) and midtropospheric rising motion (Fig. 10b) over portions of the Great Plains and Midwest during dry monsoons are consistent with enhanced precipitation. Changes in precipitation over the Great Plains appear to be more directly linked to the monsoon anticyclone than to changes in the frequency of occurrence of the Great Plains low-level jet (LLJ) or in the intensity of the moisture transport over the Great Plains (see Fig. 17 in HYW97). While the anomalies shown in Figs. 8–10 are generally in the opposite sense for wet and dry monsoons, the difference maps (Figs. 8c, 9c, and 10c) indicate that there is a bit more amplitude in the dry composites; examination of the individual events shows that no single event is dominating the composites.

In summary, the interannual variability of the warm season precipitation regime over the United States is associated with an intensification (weakening) of the climatological-mean circulation features that organize

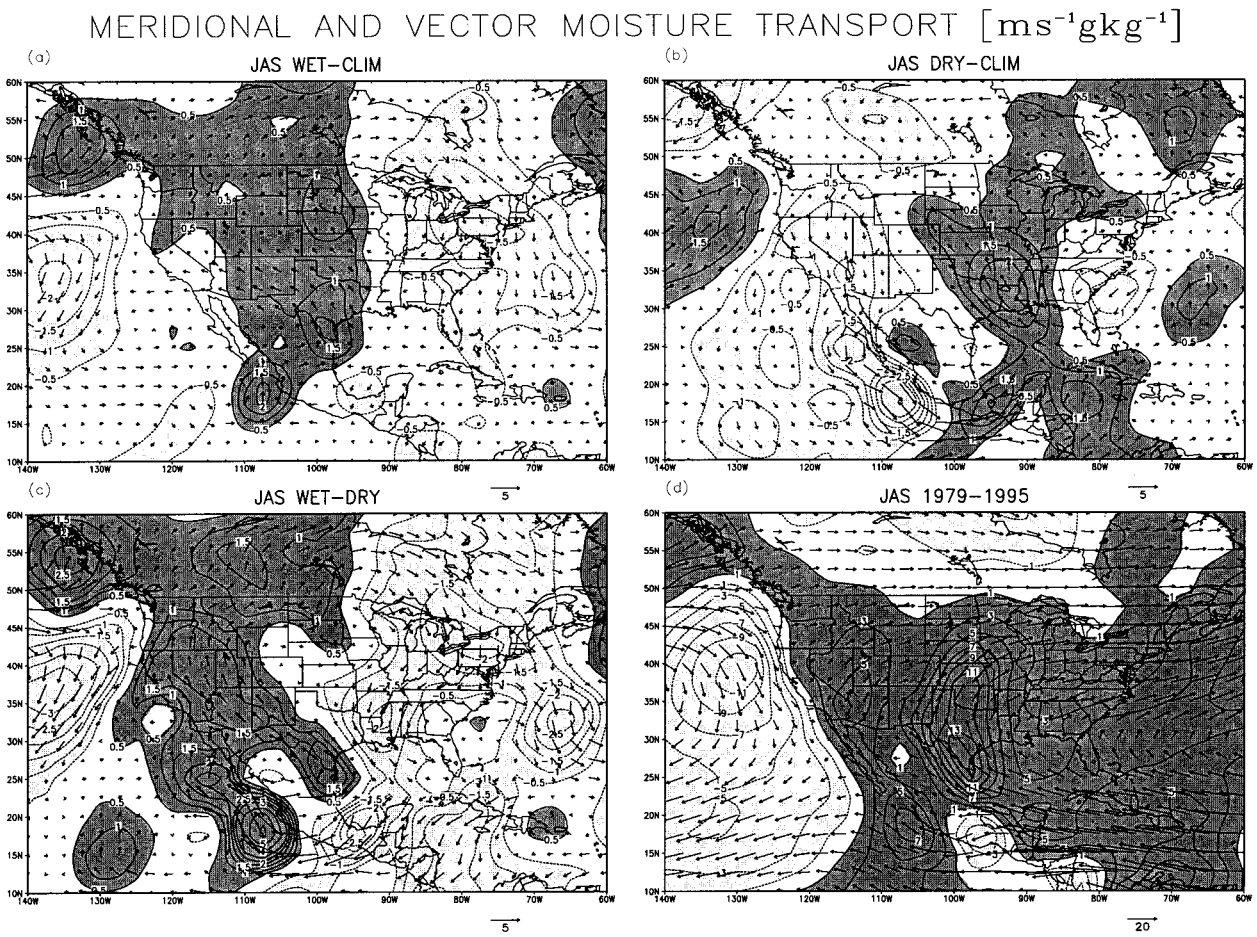

FIG. 12. JAS meridional moisture flux (shaded) and vector moisture flux (units: m s^{-1} g kg^{-1}) for (a) wet, (b) dry, (c) wet–dry, and (d) 1979–95. In (a) and (b) the fields are represented as departures from mean (JAS 1979–95) values. The fluxes are for the full vertical integral (sigma levels 1–28). In (a)–(c) the standard vector length is 5 m s^{-1} g kg^{-1} and in (d) the standard vector length is 20 m s^{-1} g kg^{-1}. In (a)–(c) the contour interval is 0.5 m s^{-1} g kg^{-1} and values of meridional flux greater than 0.5 (less than −0.5) are shaded dark (light). In (d) the contour interval is 2 m s^{-1} g kg^{-1} and values of meridional flux greater than 1 (less than −1) are shaded dark (light).

this regime, with some change in position. Of potentially greater significance for the understanding of this regime, however, is that this variability is linked to changes in the atmospheric and oceanic conditions farther south over Mexico, central America, and the eastern tropical Pacific. For example, wet monsoons in the southwestern United States are associated with suppressed precipitation in the eastern Pacific ITCZ (near 5°–10°N) and enhanced precipitation directly to the north and south of the ITCZ (Fig. 8a); the opposite phase of this pattern appears for dry monsoons (Fig. 8b). These patterns of precipitation anomalies are much more pronounced *during the spring preceding monsoon onset* (see section 4a). We note that Janowiak et al. (1995) found some disagreement in the pattern of rainfall in the east Pacific ITCZ among several satellite estimation algorithms and various other data sources; however, they found better agreement in interannual variations among the various estimates.

Latitude-pressure cross sections (120°–100°W) of the combined divergent meridional wind and pressure vertical velocity (vectors) and relative humidity (shaded) show clear evidence of a suppressed local Hadley circulation during wet monsoons (Fig. 11a) with downward motion near the climatological-mean position of the ITCZ (cf. Figs. 11a,d) and upward motion to the north and to the south. Dry (wet) conditions are found in the descending (ascending) branches as indicated by the pattern of anomalous RH. The enhanced upward motion and moist conditions near 30°N are consistent with enhanced monsoon precipitation over Arizona and New Mexico. Evidence for an enhanced local Hadley circulation during dry monsoons is less clear (Fig. 11b) because the ascent in the vicinity of the ITCZ is confined at and below 700 hPa; there is the suggestion that enhanced rainfall in the ITCZ is due to shallow convection. Large-scale descent and anomalously dry conditions are clearly evident to the north and south. Relationships between the local Hadley circulation and the large-scale forcing (e.g., SST) during the seasons preceding wet and dry monsoons are discussed further in section 4.

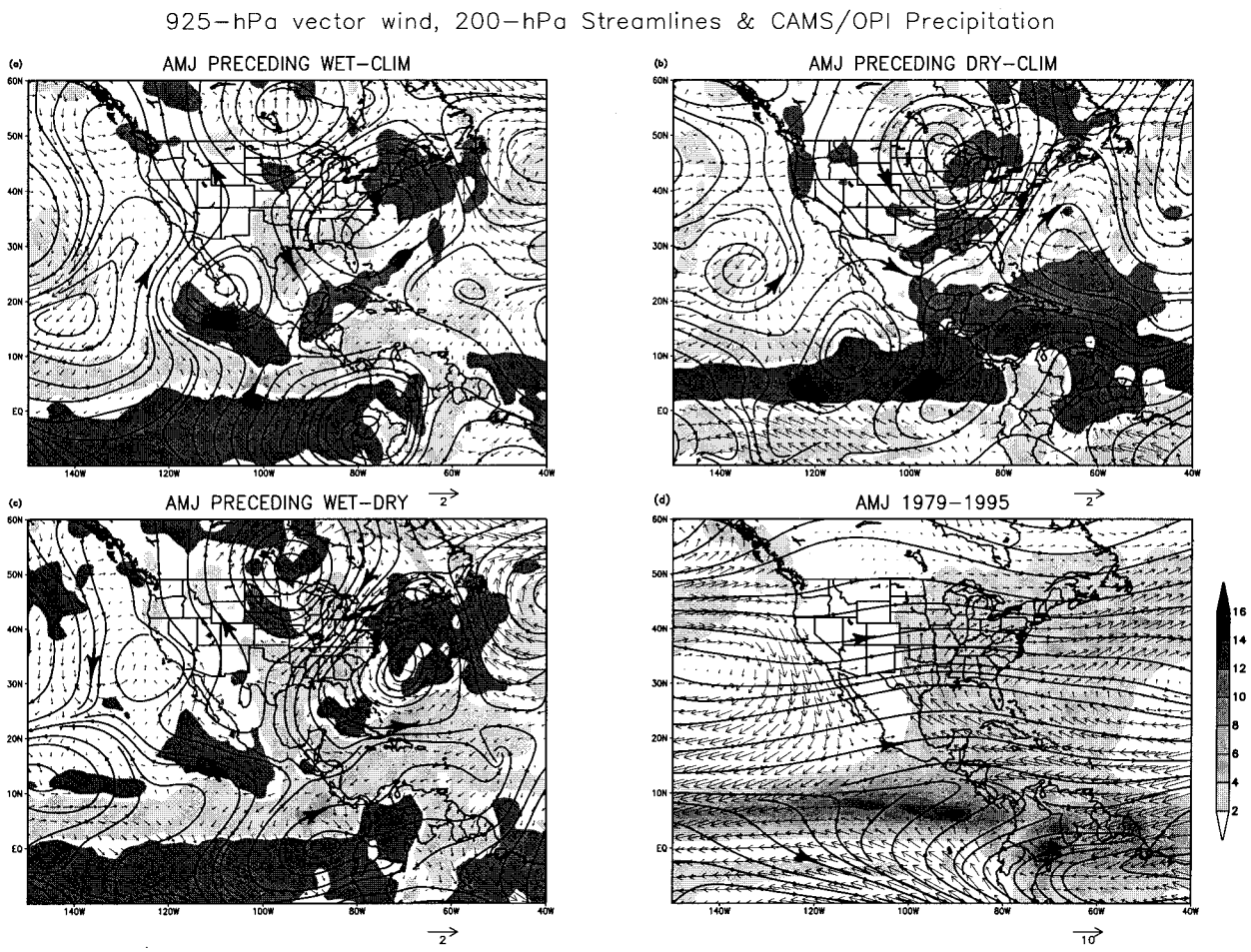

FIG. 13. April–June 925-hPa wind vectors (units: m s^{-1}), 200-hPa streamlines, and CAMS/OPI precipitation (units: mm day^{-1}) preceding (a) wet, (b) dry, (c) wet–dry, and (d) Apr–Jun (AMJ) 1979–95. In (a)–(b) the fields are represented as departures from mean (AMJ 1979–95) values. In (a)–(c) the standard vector length is 2 m s^{-1} and in (d) the standard vector length is 10 m s^{-1}. In (a)–(c), precipitation values greater than 0.25 mm day^{-1} (less than -0.25 mm day^{-1}) are shaded dark (light).

c. Moisture transport

The mean (JAS 1979–95) vertically integrated moisture transport (Fig. 12d) bears close resemblance to the low-level wind field (Fig. 8d) due to the large specific humidity at low levels. The strongest flux onto the continent occurs at low levels below 850 hPa over the south central United States and northeastern Mexico in the vicinity of the Great Plains LLJ. Higgins et al. (1996b) showed that the moisture transport in the NCEP–NCAR Reanalysis during the summer months compares favorably to rawinsonde data, though there are some significant regional differences, particularly along the Gulf Coast. Strong southward flux associated with the large-scale circulation of the east Pacific anticyclone occurs off the west coast of the United States and Mexico. The flux vectors over the Mexican plateau tend to be easterly and are noticeably smaller than in neighboring regions to the east and west, indicating little transport of moisture across Mexico at low levels. The onshore transport of moisture from the Gulf of California into southwest Arizona is relatively weak. Numerous authors have attempted to identify the primary source of moisture for the summer rains over the southwestern United States (e.g., Bryson and Lowry 1955; Rasmusson 1967; Hales 1972, 1974; Sellers and Hill 1974; Douglas et al. 1993; Douglas 1995). Schmitz and Mullen (1996) and HYW97 examined the relative importance of the Gulf of Mexico, the Gulf of California, and the eastern tropical Pacific as moisture sources for the desert Southwest using European Centre for Medium-Range Weather Forecasts analyses and NCEP–NCAR Reanalysis data, respectively. In both studies, it was found that most of the moisture at lower levels (below 850 hPa) over the desert Southwest arrives from the northern Gulf of California while most of the moisture at middle and upper levels (above 850 hPa) comes from the Gulf of Mexico. However, it remains to be determined whether the precipitation in the Southwest is linked to the moisture below 850 hPa or above 850 hPa, and then which source is feeding those levels.

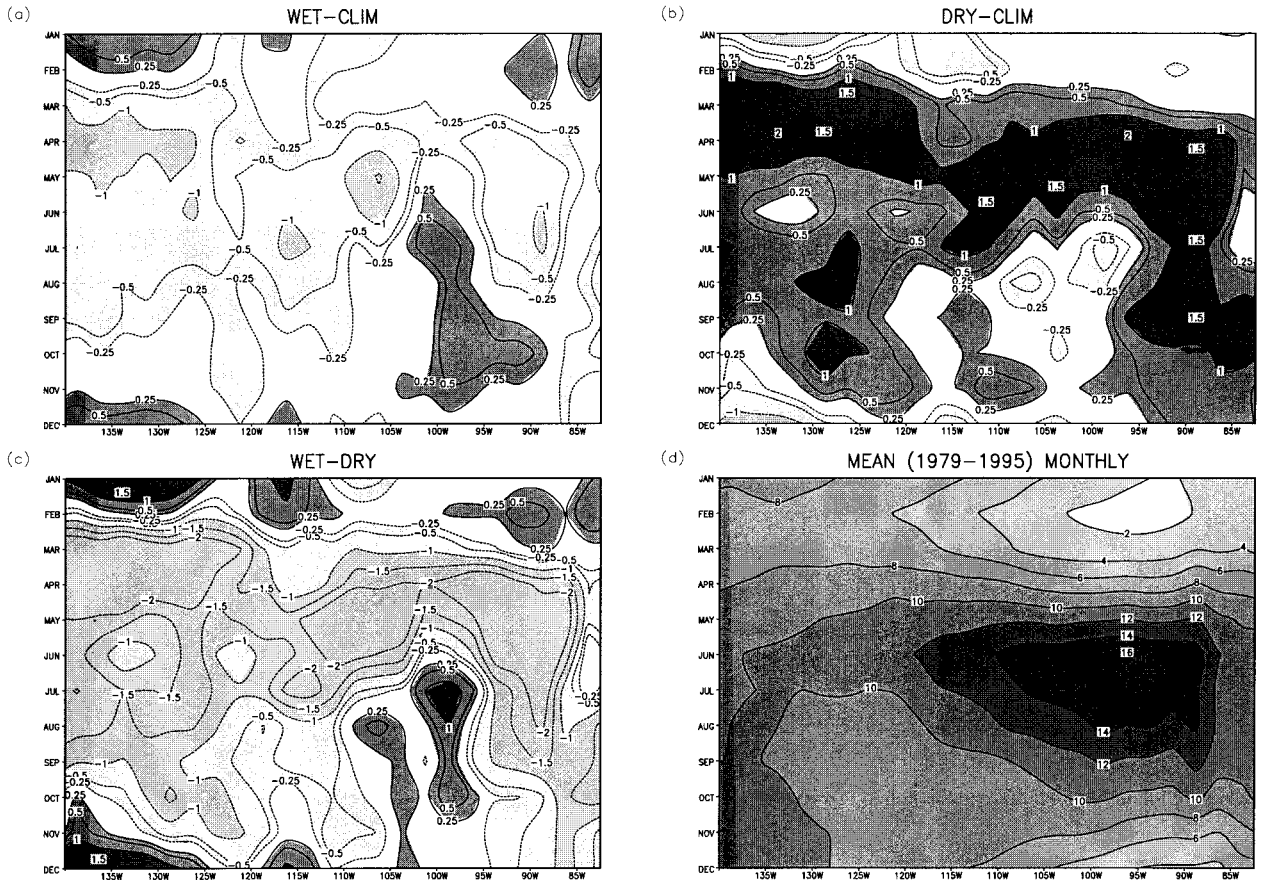

FIG. 14. Time–longitude sections of the 3-month running mean of CAMS/OPI precipitation (units: mm day^{-1}) in the ITCZ (5°–10°N) for (a) wet, (b) dry, (c) wet–dry, and (d) the mean (1979–95) annual cycle. In (a) and (b) the fields are represented as departures from mean (1979–95) monthly values. In (a)–(c) the contour interval is 0.5 mm day^{-1} (to which the 0.25 mm day^{-1} contour has been added) and positive (negative) values are shaded dark (light). In (d) the contour interval is 2 mm day^{-1} and values greater than 2 mm day^{-1} are shaded.

Wet monsoons (Fig. 12a) are associated with a continental-scale anticyclonic circulation in the anomalous transport featuring enhanced meridional transport to the west and suppressed meridional transport to the east. In the Southwest the anomalous transport is mainly from the southeast, suggesting an increased role of moisture from the western Gulf of Mexico. Dry monsoons (Fig. 12b) feature a more localized enhancement of the moisture transport from the Gulf of Mexico to the south-central United States. Anomalous westerly transport originating over the eastern tropical Pacific appears to be linked to the moisture pipeline extending from the Gulf of Mexico. Both the wet and dry composites show a center of anomalous transport to the southwest of Mexico (near 17.5°N, 107.5°W) that warrants further investigation. In the western United States the anomalous transports are generally quite weak. Of the two fields that compose the moisture flux vector, it is mostly the velocity (and not the moisture) that changes during wet and dry monsoons. Precipitable water anomalies are relatively small compared to mean values indicating that anomalous transports are mainly due to winds.

4. Changes in the eastern Pacific ITCZ cold tongue complex

a. Intensity of ITCZ precipitation

The changes in ITCZ precipitation that occur during wet and dry monsoons (see section 3b, Fig. 8) are larger and more coherent during the spring preceding the monsoon (Fig. 13), suggesting that the interannual variability of the U.S. warm season precipitation regime is linked to the season-to-season memory of the coupled atmosphere–ocean system over the eastern tropical Pacific. Because the 1983 warm episode is the strongest on record, it may dominate the composites and so has been excluded in this section.

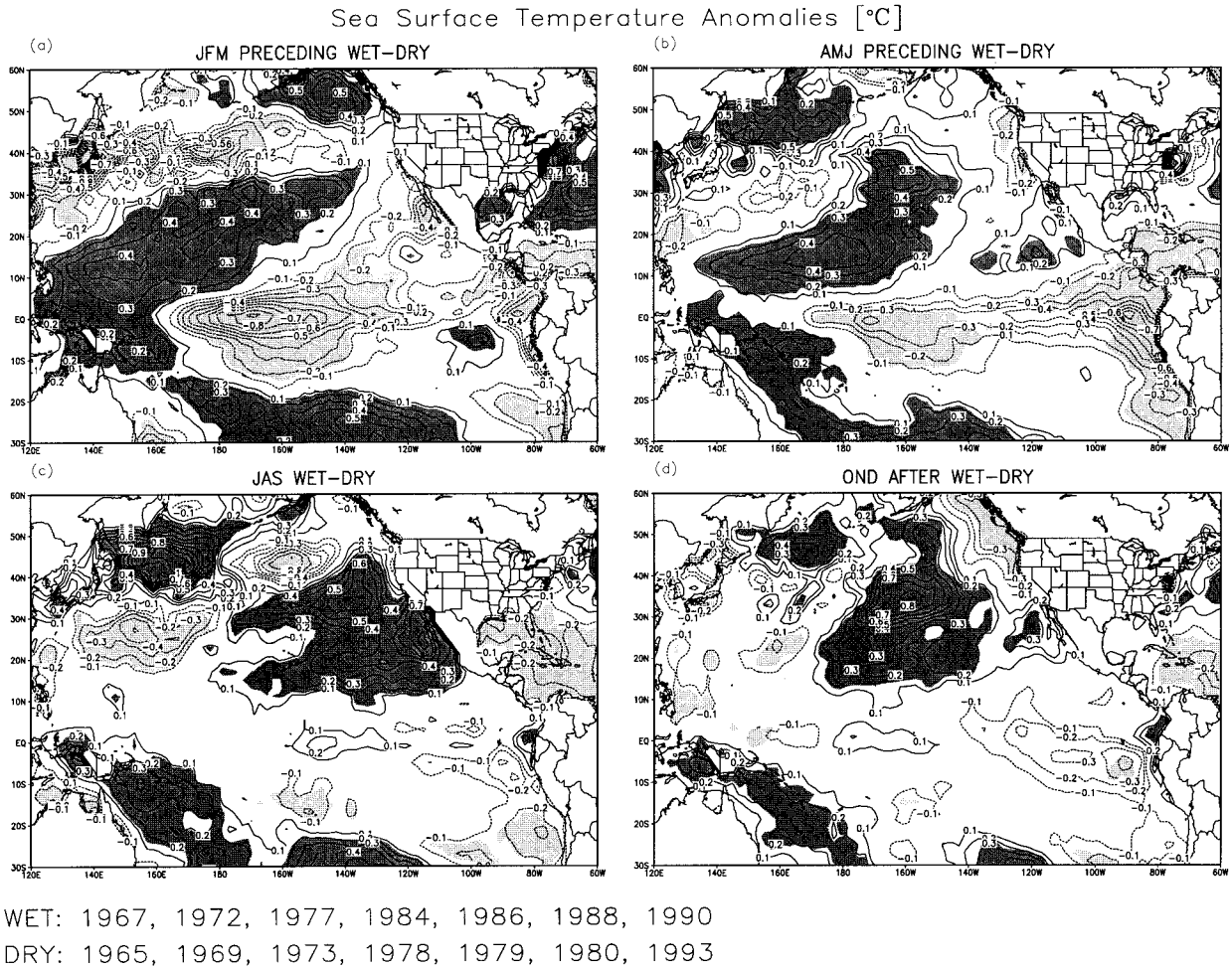

FIG. 15. Sea surface temperature anomalies (units: °C) for (a) Jan–Mar preceding wet–dry, (b) AMJ preceding wet–dry, (c) JAS during wet–dry, and (d) Oct–Dec (OND) after wet–dry. In (a)–(d) the contour interval is 0.1° C and the zero contour is omitted for clarity. The light (dark) shading indicates significance at the 90% confidence level. The events included in each composite are indicated at the bottom.

The spring preceding wet monsoons is characterized by enhanced rainfall along the southwest coast of Mexico and suppressed rainfall along the ITCZ (Fig. 13a). Focusing on the United States, we find an upper-tropospheric cyclonic anomaly centered near the southeast coast that contributes to wet conditions in the Northeast. Anomalous upper-tropospheric northerly flow and mid-tropospheric subsidence are consistent with dry conditions over portions of the southern plains, the northwestern Gulf of Mexico, and the southeastern United States. Examination of the individual years in the wet composite reveals that the subsidence and low rainfall over the southern plains/northwestern gulf are robust (present in six out of eight of the years). Successive months in the wet composite show that the region of low precipitation in the southern plains slowly shifts northward into the central plains and Midwest during the late spring and early summer as the upper-tropospheric monsoon anticyclone intensifies over the western United States.

The spring preceding dry monsoons is characterized by enhanced rainfall along the ITCZ and by suppressed rainfall to the north and south (Fig. 13b). Conditions are much drier along the west coast of Mexico, in contrast to the wet composite (Fig. 13a). Enhanced upper-level southwesterly flow is associated with wet conditions in the Gulf Coast states while enhanced southerly flow brings wet conditions to the Great Lakes region. A difference map (Fig. 13c) reflects the antisymmetry of the upper-tropospheric circulation anomalies centered near the Canadian border and off the southeast coast of the United States. An anomalous anticyclone at upper levels straddles the transition between enhanced/suppressed ITCZ rainfall near 90°W. Longitude–time sections of precipitation anomalies in the eastern Pacific ITCZ (5°–10°N) for wet (Fig. 14a) and dry (Fig. 14b) monsoons show quite clearly that departures are largest during the spring season and that they are roughly antisymmetric. For springs preceding wet monsoons, all years except 1984 are drier than normal along the ITCZ

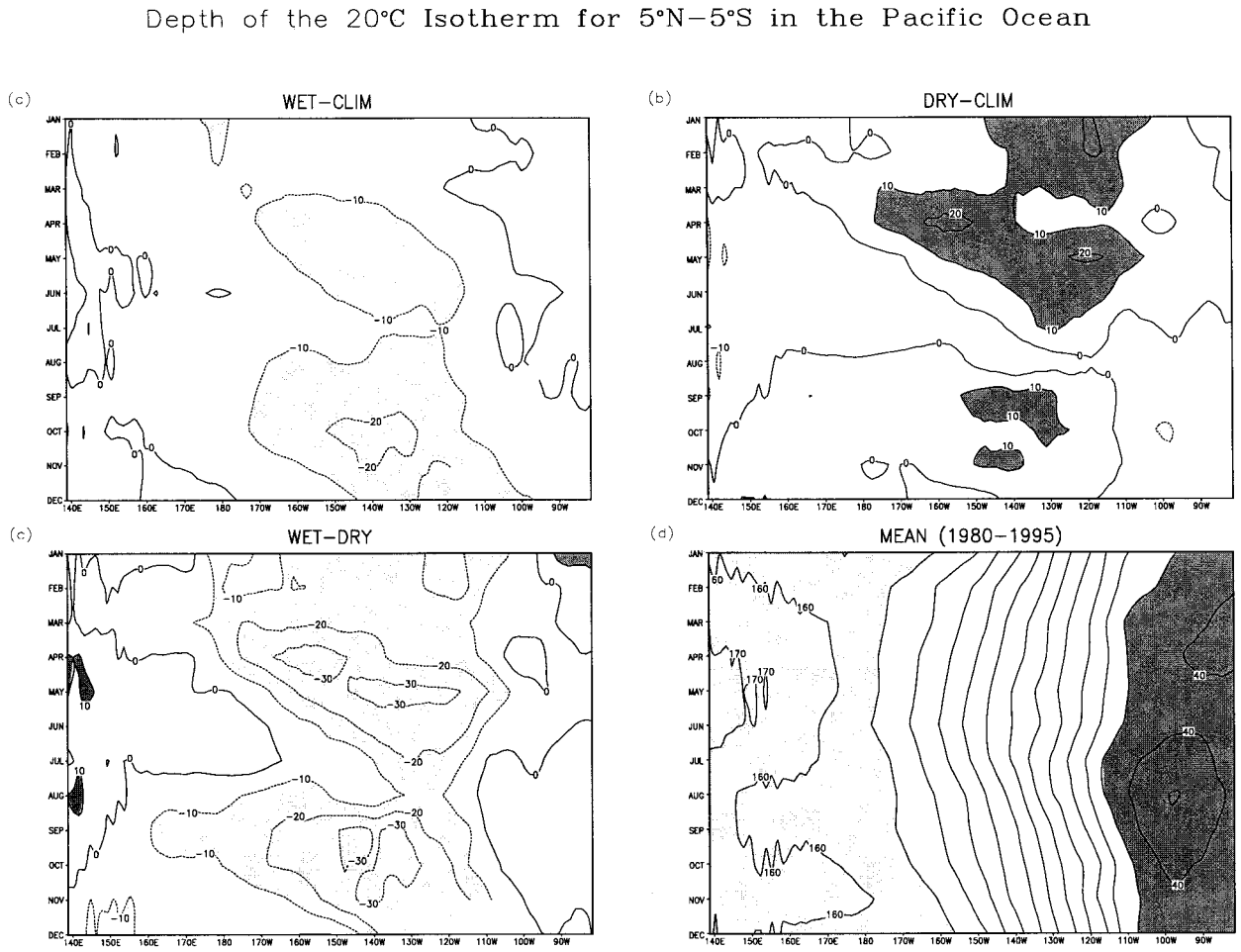

FIG. 16. Time–longitude section of the depth of the 20°C isotherm for 5°N–5°S in the Pacific Ocean for (a) wet, (b) dry, (c) wet–dry, and (d) the mean (1980–95) annual cycle. In (a)–(c) the contour interval is 10 m and values greater than 10 m (less than − 10 m) are shaded dark (light). In (d) the contour interval is 10 m and values less than 40 m (greater than 150 m) are shaded dark (light).

(5°–10°N); for springs preceding dry monsoons, all years are wetter than normal along the ITCZ.

b. SST variability in the cold tongue

Changes in the eastern Pacific ITCZ rainfall and local Hadley circulation are accompanied by consistent and coherent changes in the tropical Pacific SST and the subsurface thermal structure, particularly in the vicinity of the equatorial cold tongue. Typically, negative SST anomalies (SSTAs) in the cold tongue appear near the date line during the winter preceding the onset of wet monsoons and vice versa for dry events (Fig. 15a). These anomalies persist and gradually increase in both amplitude and areal extent over the eastern tropical Pacific during the spring (Fig. 15b). Examination of the wet and dry composites in Fig. 15 shows that the tropical anomalies are roughly antisymmetric during the winter and spring preceding the monsoon, particularly near the date line and in the far eastern tropical Pacific. The gradual eastward shift of the anomalies in the difference composite is consistent with a gradual eastward shift of the depth of the 20°C isotherm (see Fig. 16) and of subsurface thermal anomalies in the cold tongue (see Fig. 17). The anomalies in the North Pacific during winter and spring will be discussed in a follow-on study.

As the negative SSTAs intensify in the eastern tropical Pacific during the spring, positive SSTAs appear along 10°N, 140°–100°W. A comparison of Figs. 13c and 15b indicates that these SSTAs are consistent with the changes in the ITCZ and with the anomalous local Hadley circulation over the eastern tropical Pacific. Similar relationships between eastern Pacific SSTs and Arizona summer rainfall were reported by Carleton et al. (1990).

The positive SSTA over the eastern subtropical Pacific continue to strengthen during JAS (Fig. 15c), suggesting a continued relationship to changes in the ITCZ. Large positive SSTAs along the west coast of Mexico/Baja California during the summer suggest that local forcing, possibly involving some role of precipitation anomalies in governing SSTA, is important for south-

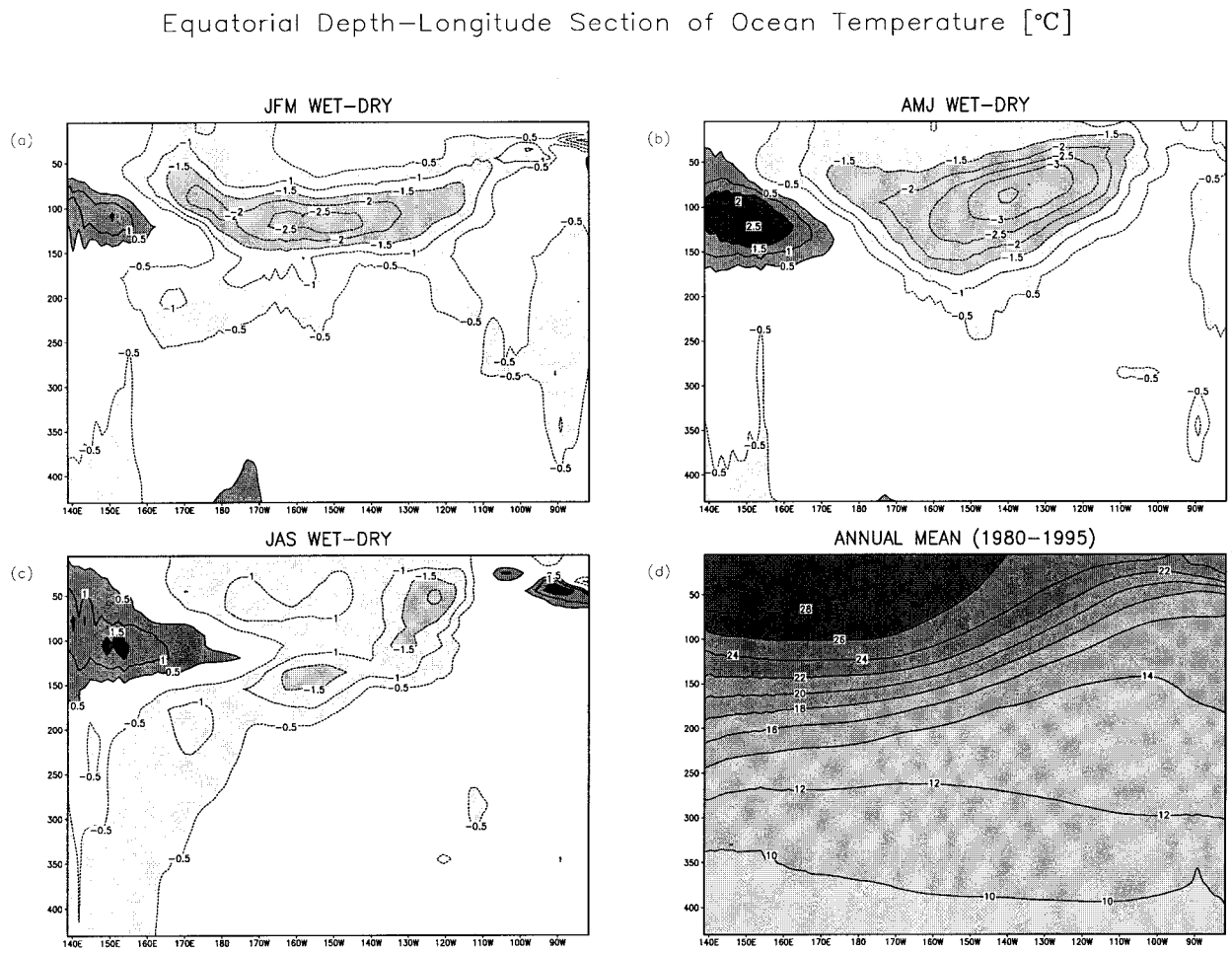

FIG. 17. Equatorial depth–longitude sections of ocean temperature represented as (a) JFM preceding wet–dry, (b) AMJ preceding wet–dry, (c) JAS during wet–dry, and (d) the mean (1980–95) annual cycle. In (a)–(c) the contour interval 0.5°C and values greater than 0.5°C (less than −0.5° C) are shaded dark (light). In (d) the contour interval is 2°C.

western U. S. precipitation. SSTAs in the cold tongue diminish considerably during the summer months (Fig. 15c), but precipitation and meridional circulation anomalies persist (Fig. 8c), particularly to the southwest of Mexico. Consideration of the full annual cycle along the southwest coast of North America indicates colder than normal conditions when it is normally cold January–March (JFM) and warmer than normal conditions when it is normally warm (JAS) reflecting an intensification of the annual cycle in local sea surface temperature during wet monsoons and vice-versa for dry monsoons.

The equatorial SSTA during the months preceding onset are consistent with temperature anomalies in the subsurface as indicated by equatorial time–longitude sections of the depth of the 20°C isotherm (Fig. 16); here negative (positive) anomalies indicate relatively cold (warm) water in the upper layers of the ocean associated with a shallowing (deepening) of the thermocline. Equatorial depth–longitude sections of ocean temperature (Fig. 17) show anomalously cold (warm) water in the upper layers of the eastern tropical Pacific during the winter preceding wet (dry) monsoons (Fig. 17a). During the spring and summer the anomalies slowly shift eastward, with some tendency for a gradual surfacing (Figs. 17b,c); this process continues into the autumn after the monsoon (not shown). Consideration of the anomalous local Hadley circulation discussed in section 4a leads us to speculate that the cooling along the equator prior to wet monsoons is due to a shallowing of the thermocline or to an upwelling and/or entrainment in response to the strengthening of the lower-tropospheric southerly winds feeding into the rapidly developing NAMS; anomalous conditions in the opposite sense prevail prior to dry monsoons. It is important to note that amplitudes of the equatorial SSTA in Fig. 15 and the surface temperatures in Fig. 17 do not match because the datasets cover different periods.

It is important to recognize that the composites in this study include many years that have not traditionally

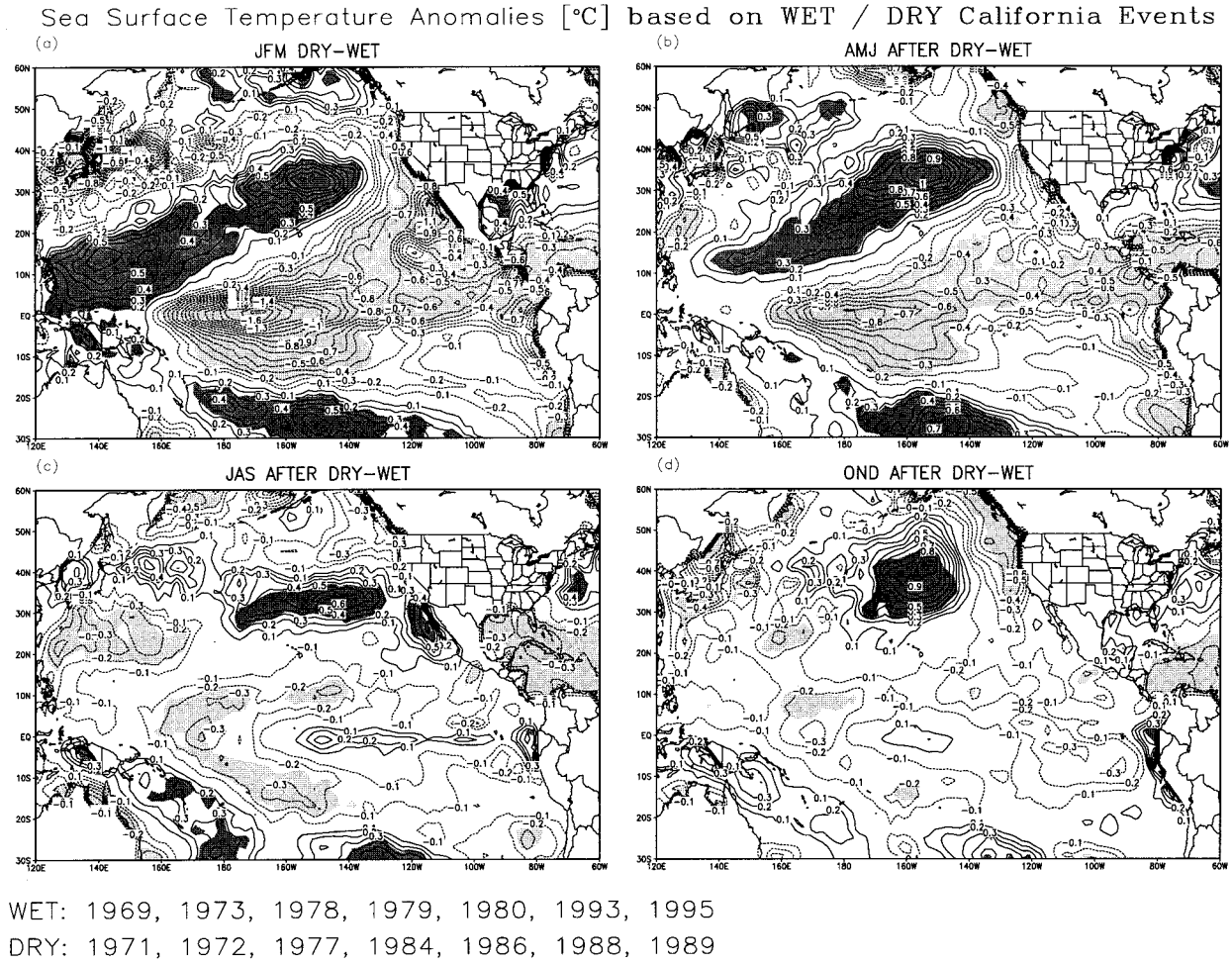

FIG. 18. Sea surface temperature anomalies (units: °C) based on southern California extreme events for (a) JFM during dry–wet, (b) AMJ after dry–wet, (c) JAS after dry–wet, and (d) OND after dry–wet. In (a)–(d) the contour interval is 0.1°C, positive (negative) values are shaded dark (light), and the zero contour is omitted for clarity. The light (dark) shading indicates significance at the 90% confidence level. The events included in each composite are indicated on the bottom.

been associated with either phase of ENSO (recall that 1983 was removed from the composites). The consistency between temperature anomalies in the subsurface, SSTA, and circulation anomalies in the eastern tropical Pacific leads us to suggest the possibility of a low-frequency control on the monsoon, not necessarily directly forced by ENSO but possibly modulated by it; the exact nature of this control is the subject of our follow-on investigations.

c. Relationships to precipitation in the preceding winter

In a recent study, Mo and Higgins (1998) examined California floods and droughts during the cold season using the precipitation dataset of HJY96. As an application of their results, we computed area mean precipitation over southern California (all grid points from 32°–38°N to the coast, 115° W) for each JFM during the period 1963–95 and stratified wet and dry events using a similar type of classification scheme to the one discussed in section 2b. Comparison of the wet (dry) California winters to the dry (wet) southwest monsoons shows 5 (6) yr in common out of a total of 8 in each case; recall that wet southwest monsoons are preceded by a dry southwest during the preceding winter and vice versa (see Fig. 3 and section 4c). The California extreme events were used to obtain the SSTA composites shown in Fig. 18. A comparison to Fig. 15 shows many similarities. During the winter the patterns of SSTA are quite similar in each case, though the local significance is higher in Fig. 18a because we have keyed to California precipitation during JFM. During the summer the patterns of SSTA near the immediate west coast of North America are similar, but the local significance is higher in Fig. 15c because we have keyed to monsoon rainfall

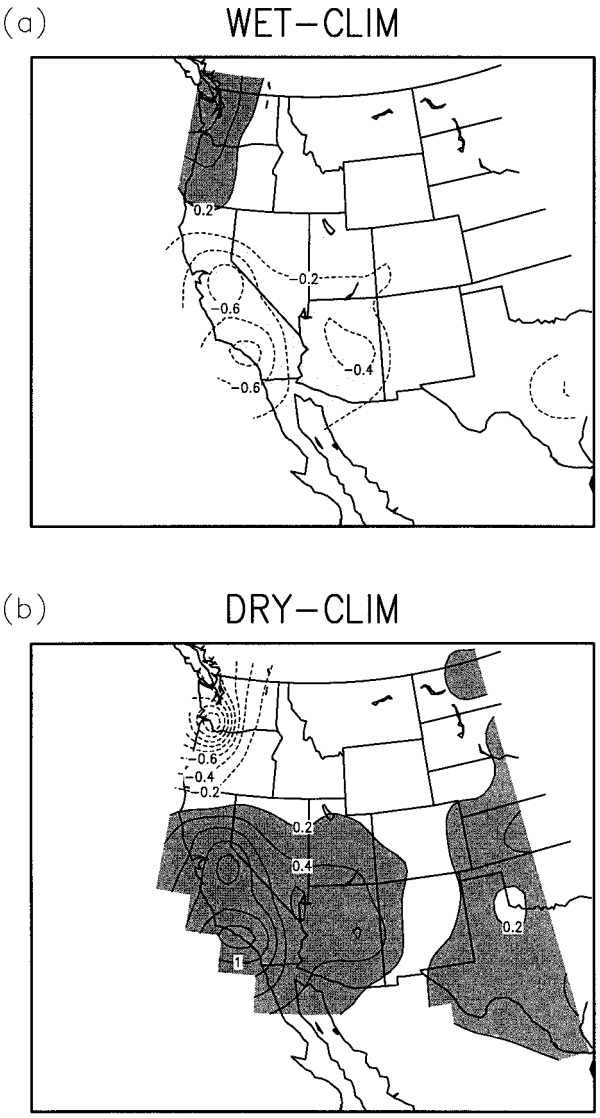

FIG. 19. Maps of observed precipitation anomalies (units: mm day^{-1}) represented as the composite mean (day −180–day −90) preceding (a) wet and (b) dry monsoons. In (a) and (b) the precipitation is represented as departures from composite mean (1963–94) daily values, the contour interval is 0.2 mm day^{-1}, and values greater than 0.2 mm day^{-1} (less than −0.2 mm day^{-1}) are shaded dark (light).

during JAS. Thus, whether we key on extreme southern California winters or on extreme southwest monsoon summers, we obtain similar SSTA composites. Overall, this is suggestive of an important relationship between California precipitation during the winter and the subsequent summer monsoon, with the long-term ''memory'' imparted, at least in part, through the SSTA. In a follow-on study we will show that much of this memory originates with the North Pacific SSTA.

Maps of the composite mean (day −180 to day −90; roughly JFM) precipitation for wet (Fig. 19a) and dry (Fig. 19b) monsoons show that wet (dry) southwest monsoons are preceded by winters characterized by dry (wet) conditions in the Southwest and wet (dry) conditions in the Pacific Northwest (also compare to Fig. 3). This relationship between rainfall in the southwest and in the Pacific Northwest during the winter preceding monsoon onset is explored further in Fig. 20, which shows a comparison of precipitation anomalies from the PI (solid line) and from the Pacific Northwest (44°–48°N, 125°–120°W, dot-dashed line) for the period from day −180 to day −90 prior to monsoon onset; note that the PI can be viewed as a proxy for California rainfall as well since rainfall anomalies in these two regions tend to be in phase during the winter preceding the monsoon and during the summer monsoon itself. Precipitation anomalies in the Southwest and in the Pacific Northwest are in the opposite sense in 23 of the 32 winter periods; the out-of-phase relationship holds for most of the winters preceding wet and dry monsoons. We note that the tendency for a phase reversal between the Southwest and the Pacific Northwest is preserved when we key to rainfall in the Pacific Northwest (not shown). These results are also consistent with those of Mo and Higgins (1998), who found a similar pattern in connection with California floods and droughts during the cold season.

Spatial maps for wet and dry monsoons (Fig. 21) show that the southwestern precipitation anomalies are embedded in a large-scale southwest to northeast band. Changes in the large-scale low-level flow and the upper-tropospheric circulation features are broadly consistent with these precipitation anomalies. Prior to wet monsoons the west coast of the United States is dominated by anomalous ridging through the depth of the troposphere consistent with wet onshore flow in the Pacific Northwest and dry offshore flow over California and the desert Southwest (Fig. 21a). The eastern two-thirds of the nation is dominated by an upper-tropospheric cyclonic anomaly and midtropospheric subsidence leading to deficit precipitation at most locations (except over Florida and portions of the Northeast). Tropospheric anomalies during the winter preceding dry monsoons are generally in the opposite sense, leading to dry conditions over the Pacific Northwest and wet conditions over the Southwest and most of the eastern United States (Fig. 21b). These patterns of precipitation and circulation anomalies are consistent with those discussed by Carleton et al. (1990), who found that wetter summers in Arizona tend to follow positive high-amplitude values of the Pacific–North America (PNA) teleconnection pattern during the previous winter. In these winters they found an amplified ridge over western North America and a deepened trough over the east-central North Pacific. In the winters preceding dry Arizona summers they found a more zonal pattern associated with the negative phase of the PNA. Thus, there is the suggestion that the PNA is linked to the subsequent summer circulation and rainfall of the southwestern United States. Carleton et al. (1990) also concluded that this association arises, at least in part, from memory imparted to

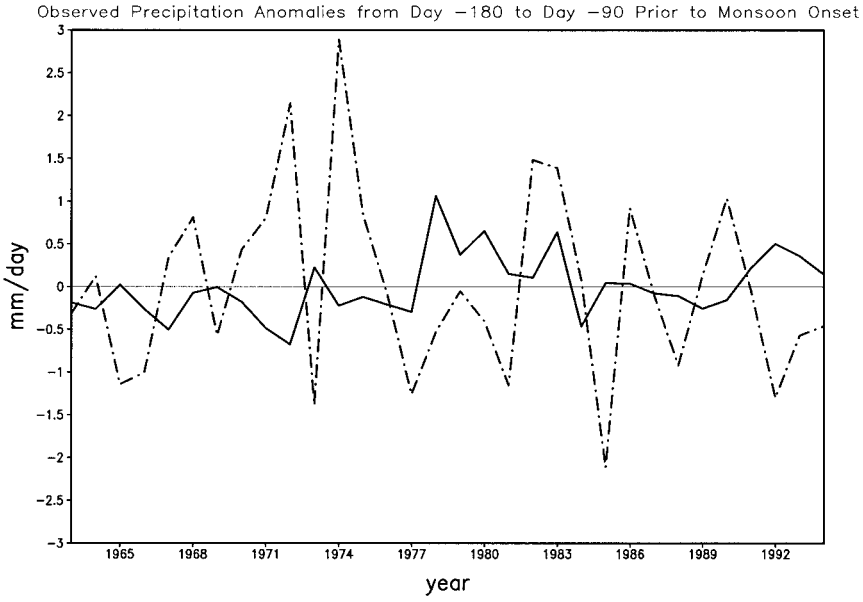

FIG. 20. A real average observed precipitation anomalies (units: mm day^{-1}) for the period from day −180–day −90 prior to monsoon onset from the PI region (solid line) and from the Pacific northwest (44°–48°N, 125°–120°W) (dot-dashed line).

the atmosphere by the accompanying pattern of Pacific SSTA during the winter and spring preceding the monsoon; the SSTA results presented in the preceding subsection (see Figs. 15 and 18) are consistent with this conclusion.

The wet and dry precipitation composites in Fig. 21 both show a three-cell pattern oriented from north to south along the West Coast; during winters preceding wet monsoons the three-cell pattern features enhanced precipitation over the Gulf of Alaska, southeastern Alaska, and the Pacific Northwest; suppressed precipitation over Southern California, Arizona, and Baja California; and enhanced precipitation over the eastern tropical Pacific. This three-cell pattern has been discussed extensively in connection with California floods and droughts during the cold season by Mo and Higgins (1998), where it was shown to be a nearly ubiquitous feature of the wintertime precipitation pattern during conditions dominated by both ENSO and intraseasonal (MJO) activity. Mo and Higgins concluded that the most important factor determining precipitation in California was the convection pattern in the eastern tropical Pacific, even during ENSO events, suggesting that local influences may sometimes dominate remote ones in controlling California precipitation. This appears to be consistent with results of Bell and Basist (1994), who maintain that roughly 80% of the variance in California rainfall is associated with the prevailing wind direction. We note that the three-cell pattern also appears in composites of various other fields such as moisture flux divergence (not shown) during winters preceding wet and dry monsoons, but no attempt has been made to separate these composites based on the ENSO, the MJO, or other tropical phenomena.

When the composites in Fig. 21 are extended to include the entire Pacific basin (Fig. 22a), we find that the band of anomalous precipitation over the southwestern United States extends southwestward across the Hawaiian Islands toward the date line. The spring composite (Fig. 22b) is consistent with the changes in the vicinity of the ITCZ cold tongue complex discussed in sections 4a and 4b. During JAS there is good agreement between precipitation anomalies (Fig. 22c) and SSTA (Fig. 15c) to the southwest of Mexico, emphasizing the potential importance of local feedbacks.

5. Summary and discussion

A daily precipitation index (PI) defined over Arizona and New Mexico was used to show that the interannual variability of the warm season precipitation regime closely mimics changes associated with the development of the NAMS. Both wet and dry monsoons exhibit a ''monsoon signal'' associated with the onset of the Arizona–New Mexico rainy season, but wet monsoons are characterized by a much longer period of heavy rainfall in the Southwest after onset. Over portions of the northern plains and northeast the differences between wet and dry monsoons are roughly as large as they are in the Southwest emphasizing the potential impact of monsoon variability on ground water and irrigation for these regions. During wet monsoons much of the central Great Plains, lower Mississippi Valley, and East Coast are drier than normal, while the Great Lakes

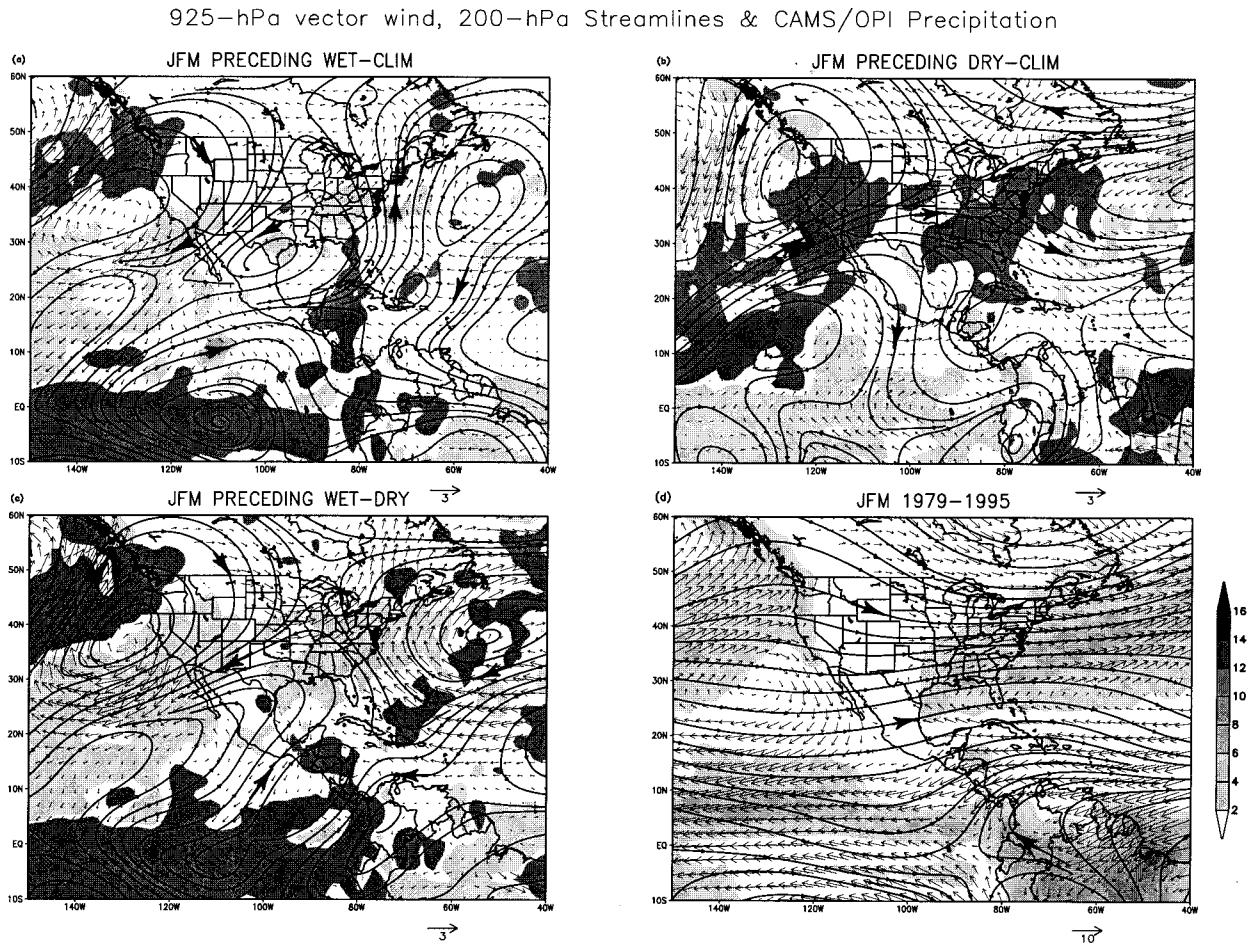

FIG. 21. January–March 925-hPa wind vectors (units: m s^{-1}), 200-hPa streamlines, and CAMS/OPI precipitation (units: mm day^{-1}) preceding (a) wet, (b) dry, (c) wet–dry, and (d) JFM 1979–95. In (a) and (b) the fields are represented as departures from mean (JFM 1979–95) values. In (a)–(c) the standard vector length is 3 m s^{-1} and in (d) the standard vector length is 10 m s^{-1}. In (a)–(c), precipitation values greater than 0.25 mm day^{-1} (less than -0.25 mm day^{-1}) are shaded dark (light).

and southern Texas are wetter than normal. During dry monsoons much of the Mississippi Valley, Ohio Valley, and mid-Atlantic are wetter than normal while portions of the Great Lakes and Northeast are drier than normal. As evidence of the continental nature of this precipitation pattern, we reiterate that the 1988 Midwest drought (1993 Midwest flood) occurred during warm seasons characterized by wet (dry) monsoons. The cellular nature of the continental-scale precipitation anomaly patterns for all types of monsoons (i.e., wet, dry, normal) seems to suggest that United States agriculture is virtually immune to entire failure.

Changes in the tropospheric circulation and moisture fields are broadly consistent with the distribution of warm season precipitation during wet and dry events. During wet monsoons the upper-tropospheric monsoon anticyclone is much stronger than normal and shifted to the northeast of its climatological mean position consistent with enhanced precipitation over Arizona and New Mexico. During dry monsoons the upper-level flow is characterized by a broad flattening and southward shift of the monsoon anticyclone consistent with an increased zonal component of the flow, suppressed precipitation in the Southwest, and enhanced precipitation in the Great Plains. The intensity of the monsoon anticyclone appears to be one of the most fundamental controls on summertime precipitation over the central United States. Our interpretation that flooding in the Midwest is related to a weakening of the monsoon anticyclone is consistent with recent work on the causes of the Midwest summertime floods of 1993 (Bell and Janowiak 1995). It should be noted, however, that the controlling factors may be reversed in some instances such that hydrologic anomalies in the Midwest may control the evolution of the monsoon. This would most likely be true when hydrologic anomalies precede monsoon onset, as was the case with the 1988 drought. In these cases the physical mechanisms may be quite different.

The interannual variability of the United States warm

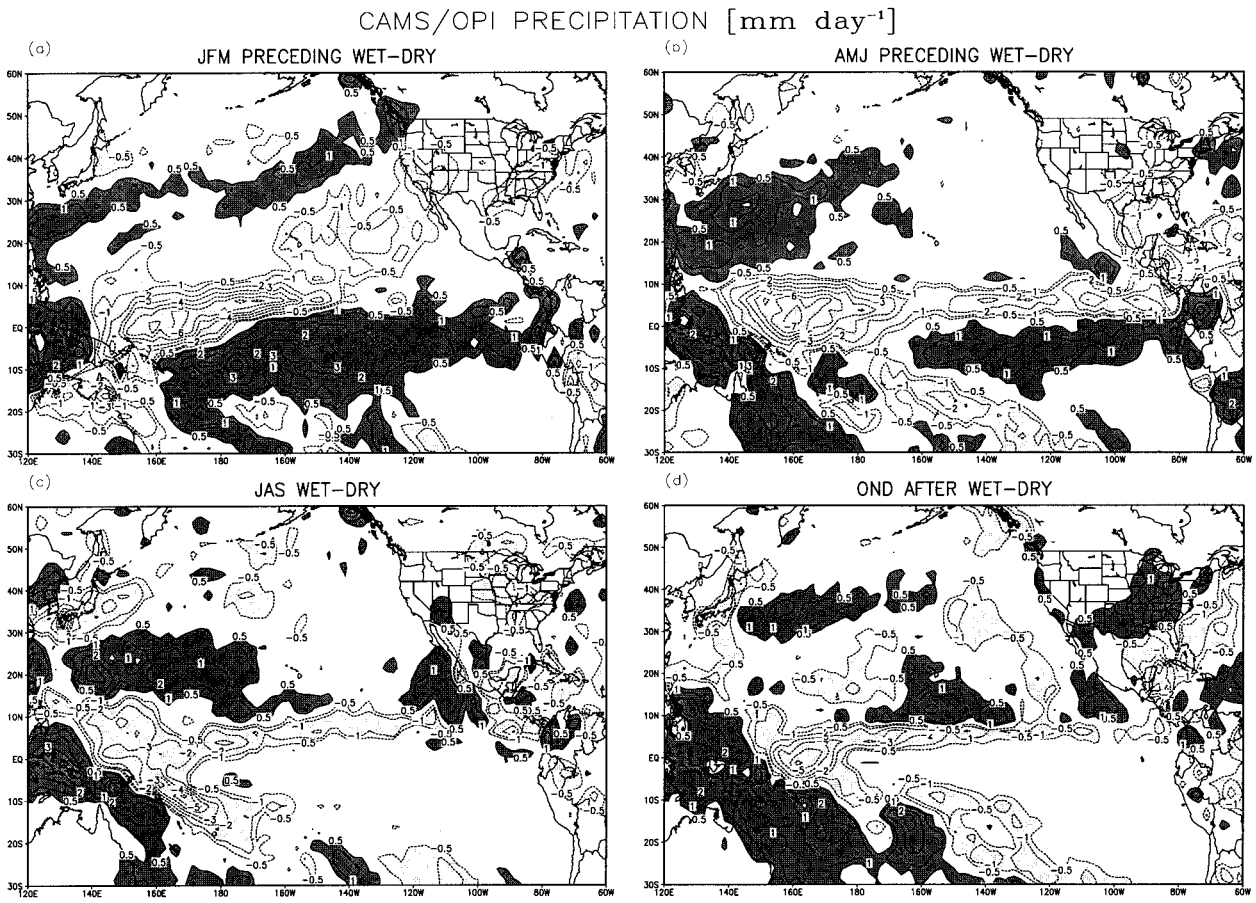

FIG. 22. CAMS/OPI precipitation (units: mm day^{-1}) represented as (a) JFM preceding wet–dry, (b) AMJ preceding wet–dry, (c) JAS preceding wet–dry, and (d) OND following wet–dry. The contour interval is 1 mm day^{-1} (to which the 0.5 mm day^{-1} contour has been added), and values greater than 0.5 mm day^{-1} (less than -0.5 mm day^{-1}) are shaded dark (light).

season precipitation regime is also linked to changes in the eastern tropical Pacific ITCZ cold tongue complex. In particular, wet monsoons appear to be associated with suppressed ITCZ rainfall and a suppressed local Hadley circulation consistent with the pattern of tropical precipitation anomalies; the opposite is true for dry monsoons. Anomalies in ITCZ precipitation and the local Hadley circulation are largest during the spring preceding the monsoon. Changes in ITCZ rainfall and the local Hadley circulation are accompanied by consistent changes in SST, particularly in the vicinity of the eastern tropical Pacific cold tongue. While SSTAs in the cold tongue typically appear during the winter preceding onset, they increase in amplitude and zonal extent during the spring. SSTAs in the cold tongue are consistent with the equatorial subsurface thermal structure of the ocean. The gradual surfacing of subsurface equatorial temperature anomalies during the spring and summer months suggests that cooling along the equator prior to wet monsoons is due to a shallowing of the thermocline or to an upwelling and/or entrainment in response to the strengthening of the southerly surface winds feeding into the rapidly developing NAMS; the opposite is true for dry monsoons. Such an argument is consistent with the anomalous local Hadley circulation, which persists through the spring and summer months. While SSTAs in the cold tongue diminish during the summer months, the precipitation and meridional circulation anomalies persist. Local feedbacks between precipitation and SST appear to be important along the West Coast during the summer months, though these feedbacks were not examined explicitly.

These results suggest that local forcing by SSTAs may be more important during the summer monsoon and that remote forcing (e.g., by SSTAs in the cold tongue or in the North Pacific) may play a catalytic and/or feedback role in the initiation of meridional circulation and precipitation anomalies during the preceding winter and spring. However, inference of causal relationships based on the evidence presented is difficult because the anomalous surface winds can induce SSTA of their own, and anomalous boundary conditions in different regions are often interrelated by way of planetary-scale atmospheric teleconnections. Studies of the atmospheric response to this anomalous boundary forcing (includes both SST and land–surface processes) using atmospheric GCMs

and/or coupled atmosphere–ocean–land GCMs are needed. In addition, field studies are required to assess and/or validate the atmospheric PBL structure above the cold tongue, the structure and intensity of the ITCZ rainfall, and air–sea fluxes in the ITCZ cold tongue complex.

Areal estimates of monthly precipitation show that winters characterized by wet (dry) conditions in the Pacific northwest and dry (wet) conditions in the Southwest tend to precede summers characterized by wet (dry) monsoons. The wintertime precipitation anomalies in the Southwest were embedded in a large-scale southwest–northeast band extending from the tropical Pacific to the eastern United States. Along the west coast of North America the three-cell pattern, discussed in connection with California floods and droughts by Mo and Higgins (1998), was prominent in the composites. The connection between wintertime precipitation along the west coast and the summer monsoon is worth pursuing further (including aspects of predictability).

Collectively, these results indicate that the interannual variability of the United States warm season precipitation regime is linked to the season-to-season memory of the coupled system over the Pacific. In particular, it would appear that prediction of SST and precipitation (e.g., in the eastern tropical Pacific), are prerequisites for successful seasonal-to-interannual prediction of warm season precipitation over extratropical North America. It is also important to recognize that the composites in this study include many years that have not traditionally been associated with either phase of ENSO (recall that 1983 was removed from the composites in section 4). This suggests the possibility of a low-frequency control on the monsoon, not necessarily directly forced by ENSO but possibly modulated by it. The search for other significant relationships linking the NAMS to the ENSO cycle and to decade-scale variability in the North Pacific will be continued in follow-on studies.

Acknowledgments. We wish to thank Tom Smith for the sea surface temperature and subsurface ocean temperature data, John Janowiak and Pingping Xie for the CAMS/OPI precipitation data, and the Environmental Modeling Center Reanalysis Team for the NCEP–NCAR Reanalysis data. The authors are also indebted to John Janowiak and Chester Ropelewski for comments that have helped to substantially improve the manuscript and to Eugene Rasmusson, Dan Cayan, Kelly Redmond, Vernon Kousky, and Gerry Bell for insightful discussions. This work was partially supported by the NOAA Office of Global Programs under the GEWEX Continental-Scale International Project (GCIP) and by Interagency Agreement S-41367-F under the authority of NASA/GSFC.

REFERENCES

Augustine, J. A., and F. Caracena, 1994: Lower-tropospheric precursors to nocturnal MCS development over the central United States. *Wea. Forecasting,* **9,** 116–135.

Baden-Dangon, A., C. E. Dorman, M. A. Merrifield, and C. D. Winant, 1991: The lower atmosphere over the Gulf of California. *J. Geophys. Res.,* **96,** 16 877–16 896.

Bell, G. D., and A. N. Basist, 1994: The global climate of December 1992–February 1993. Part I: Warm ENSO conditions continue in the tropical Pacific; California drought abates. *J. Climate,* **7,** 1581–1605.

——, and J. E. Janowiak, 1995: Atmospheric circulation associated with the Midwest floods of 1993. *Bull. Amer. Meteor. Soc.,* **76,** 681–695.

Bonner, W. D., 1968: Climatology of the low-level jet. *Mon. Wea. Rev.,* **96,** 833–850.

——, and J. Paegle, 1970: Diurnal variations in boundary layer winds over the south-central United States in summer. *Mon. Wea. Rev.,* **98,** 735–744.

Bryson, R. A., and W. P. Lowry, 1955: The synoptic climatology of the Arizona summer precipitation singularity. *Bull. Amer. Meteor. Soc.,* **36,** 329–339.

Carleton, A. M., D. A. Carpenter, and P. J. Weser, 1990: Mechanisms of interannual variability of the southwest United States summer rainfall maximum. *J. Climate,* **3,** 999–1015.

Douglas, M. W., 1995: The summertime low-level jet over the Gulf of California. *Mon. Wea. Rev.,* **123,** 2334–2347.

——, R. A. Maddox, K. Howard, and S. Reyes, 1993: The Mexican monsoon. *J. Climate,* **6,** 1665–1677.

Hagemeyer, B. C., 1991: A lower-tropospheric climatology for March through September: Some implications for thunderstorm forecasting. *Wea. Forecasting,* **6,** 254–270.

Hales, J. E., Jr., 1972: Surges of maritime tropical air northward over the Gulf of California. *Mon. Wea. Rev.,* **100,** 298–306.

——, 1974: Southwestern United States summer monsoon source—Gulf of Mexico or Pacific Ocean? *J. Appl. Meteor.,* **13,** 331–342.

Helfand, H. M., and S. D. Schubert, 1995: Climatology of the Great Plains low-level jet and its contribution to the continental moisture budget of the United States. *J. Climate,* **8,** 784–806.

Higgins, R. W., J. E. Janowiak, and Y. Yao, 1996a: A gridded hourly precipitation data base for the United States (1963–1993). NCEP/Climate Prediction Center Atlas No. 1, 47 pp.

——, K. C. Mo, and S. D. Schubert, 1996b: The moisture budget of the central United States in spring as evaluated in the NCEP/NCAR and the NASA/DAO reanalyses. *Mon. Wea. Rev.,* **124,** 939–963.

——, Y. Yao, E. S. Yarosh, J. E. Janowiak, and K. C. Mo, 1997a: Influence of the Great Plains low-level jet on summertime precipitation and moisture transport over the central United States. *J. Climate,* **10,** 481–507.

——, ——, and X. Wang, 1997b: Influence of the North American monsoon system on the U.S. summer precipitation regime. *J. Climate,* **10,** 2600–2622.

Janowiak, J. E., P. A. Arkin, P. Xie, M. L. Morrissey, and D. R. Legates, 1995: An examination of the east Pacific ITCZ rainfall distribution. *J. Climate,* **8,** 2810–2823.

Ji, M., A. Leetma, and J. Derber, 1995: An ocean analysis system for seasonal to interannual climate studies. *Mon. Wea. Rev.,* **123,** 460–481.

Johnson, A. M., 1976: The climate of Peru, Bolivia and Ecuador. *Climates of Central and South America,* W. Schwerdtfeger and H. E. Landsberg, Eds., World Survey of Climatology, Vol. 12, Elsevier, 147–218.

Kalnay, E., and Coauthors, 1996: The NCEP/NCAR 40-year Reanalysis Project. *Bull. Amer. Meteor. Soc.,* **77,** 437–471.

Maddox, R. A., 1980: Mesoscale convective complexes. *Bull. Amer. Meteor. Soc.,* **61,** 1374–1387.

Mitchell, M. J., R. A. Arritt, and K. Labas, 1995: A climatology of

the warm season Great Plains low-level jet using wind profiler observations. *Wea. Forecasting*, **10,** 576–591.

Mo, K. C., and R. W. Higgins, 1996: Large-scale atmospheric moisture transport as evaluated in the NCEP/NCAR and the NASA/DAO reanalyses. *J. Climate*, **9,** 1531–1545.

——, and ——, 1998: Tropical influences on California precipitation. *J. Climate*, **11,** 412–430.

——, J. N. Paegle, and R. W. Higgins, 1997: Atmospheric processes associated with summer floods and droughts in the central United States. *J. Climate*, **10,** 3028–3046.

Mock, C. J., 1996: Climatic controls and spatial variations of precipitation in the western United States. *J. Climate*, **9,** 1111–1125.

Negri, A. J., R. F. Adler, E. J. Nelkin, and G. J. Huffman, 1994: Regional rainfall climatologies derived from special sensor microwave imager (SSM/I) data. *Bull. Amer. Meteor. Soc.*, **75,** 1165–1182.

Okabe, I. T., 1995: The North American monsoon. Ph.D. dissertation, University of British Columbia, Vancouver, British Columbia, Canada, 146 pp.

Parrish, D. F., and J. C. Derber, 1992: The National Meteorological Center's spectral statistical interpolation analysis system. *Mon. Wea. Rev.*, **120,** 1747–1763.

Rasmusson, E. M., 1967: Atmospheric water vapor transport and the water balance of North America: Part I. Characteristics of the water vapor flux field. *Mon. Wea. Rev.*, **95,** 403–426.

Schmitz, J. T., and S. Mullen, 1996: Water vapor transport associated with the summertime North American monsoon as depicted by ECMWF analyses. *J. Climate*, **9,** 1621–1634.

Sellers, W. D., and R. H. Hill, 1974: *Arizona Climate, 1931–1972*. The University of Arizona Press, 616 pp.

Smith, T. M., R. W. Reynolds, R. E. Livezey, and D. C. Stokes, 1996: Reconstruction of historical sea surface temperatures using empirical orthogonal functions. *J. Climate*, **9,** 1403–1420.

Starr, V. P., J. P. Peixoto, and H. R. Crisi, 1965: Hemispheric water balance for the IGY. *Tellus*, **17,** 463–472.

Stensrud, D. J., R. L. Gall, S. L. Mullen, and K. W. Howard, 1995: Model climatology of the Mexican monsoon. *J. Climate*, **8,** 1775–1794.

Tang., M., and E. R. Reiter, 1984: Plateau monsoons of the Northern Hemisphere: A comparison between North America and Tibet. *Mon. Wea. Rev.*, **112,** 617–637.

Wallace, J. M., 1975: Diurnal variations in precipitation and thunderstorm frequency over the conterminous United States. *Mon. Wea. Rev.*, **103,** 406–419.

Xie, P., and P. A. Arkin, 1996: Analyses of global monthly precipitation using gauge observations, satellite estimates, and numerical model predictions. *J. Climate*, **9,** 840–858.

——, and ——, 1998: Global monthly precipitation estimates from satellite-observed outgoing longwave radiation. *J. Climate*, **11,** 137–164.